Molecular compositions of myelin that restrict localization of axonal proteins to the nodal region in myelinated fibers

Tomoko Ishibashi

Doctor of Philosophy

Department of Physiological Sciences
School of Life Science
The Graduate University for Advanced Studies

2001 (School Year)

Contents

Discussion

Materials and Methods

Summary

Ion fluxes in mammalian myelinated axons are restricted to the nodes of Ranvier, where, in particular, voltage-gated Na^+ channels are clustered at a high density. The node of Ranvier is separated from the internode by two distinct domains of the axolemma, the paranode and the juxtaparanode. Each axonal domain is characterized by the presence of specific protein complexes. Shaker-type K^+ channels are concentrated at the juxtaparanode, one side of which is delimited by paranodal axo-glial junction. Although oligodendrocytes and/or myelin membranes are believed to play some instructive roles in the organization of axonal domains, the mechanisms leading to their localized distribution are not well understood. In this thesis, I focused on the involvement of myelin membranes in this domain organization and molecular mechanisms in formation of the paranodal junction. I examined the distribution of axonal components in mice under normal and pathological conditions. From these analyses, I found that each of the Na^+ and K^+ channels required myelin membranes in a distinct manner. Neither compact myelin nor paranodal junction is essential for initial clustering of Na^+ channels, even though oligodendrocytes or some glial contact may regulate the initial clustering. While both compact myelin and paranodal junction are required for the nodal maturation. For K^+ channel clusters, in contrast, compact myelin is essential for the initial clustering as well as for maintenance of the clusters, but the clusters can be formed independently of the paranodal junction. Proper localization of K^+ channel clusters requires both paranodal junction and compact myelin. Furthermore, I demonstrate that myelin protein CD9 is concentrated at the paranode and that the mice lacking either CD9 or sulfatide show paranodal abnormality and alteration

of axonal protein localizations. These results indicate that both sulfatide and CD9 have critical roles on the formation of the paranodal junction as well as axonal domain organization.

Introduction

In the mammalian nervous system, myelin membranes are formed by oligodendrocytes in central nervous system (CNS) and by Schwann cells in peripheral nervous system (PNS). These membranes serve as an axonal insulator that facilitates transmission of nerve impulses through saltatory conduction. It has been shown recently that the myelin membrane functions not only to insulate the axons, but segregates the axonal surface into four discrete functional domains, consisting of the internode, juxtaparanode, paranode, and the node of Ranvier (Fig. 1, for review; Salzer 1997; Pedraza, et al., 2001). At the paranode, the interface between the lateral loops and the axonal membrane exhibits a row of 10-15 nm regularly spaced densities, referred as the transverse band (Fig. 1, Hirano et al., 1982). Voltage-gated Na^+ and K^+ channels are localized in the distinct subcellular domains in the myelinated nerve fiber. Specifically, Na^+ channels are clustered at high densities in the nodes of Ranvier, whereas shaker-type K^+ channels α subunits (Kv1.1, Kv1.2) and their β subunit Kvβ2 are concentrated at the juxtaparanodal regions (Fig. 1, Wang et al., 1993; Rasband et al., 1998; Vabnick et al., 1999). Specific targeting, clustering, and maintenance of these channels in their respective domains are essential to achieve a high conduction velocity. Although oligodendrocytes and/or myelin membranes are believe to play some instructive roles in organization of these domains, the exact mechanisms that mediate these distributional changes remain largely undefined. In this thesis, I focused my interest on the involvement of myelin sheaths in this axonal domain formation. This thesis consists of two chapters, in which I address the following two questions. Which myelination process is responsible for organization of the axonal domains?

(Chapter I) What kinds of myelin components are involved in this domain formation?

(Chapter II)

Chapter I

Introduction

Which myelination process is responsible for organization of axonal domains?

In the past few years, numbers of studies have attempted to clarify the roles of myelin sheaths on the axonal domain formation. However, it is still controversial how the interaction between myelin-forming cells and axons is involved in this process. One report suggested that a protein secreted by oligodendrocytes induced Na^+ channel clustering at a regular interval corresponding to the future internodal distance without any glial contact in cultured CNS neurons (Kaplan et al., 1997). Several studies have also described that Na^+ channel clustering without any direct glial association both in the CNS and PNS axons (Deerinck et al., 1997; Lambert et al., 1997). In contrast, the results from experiments on sciatic nerves during both development (Vabnick et al., 1996) and remyelination (Dugandzija-Novakovic et al., 1995) suggest that either Schwann cell contact or myelination is required for nodal Na^+ channel clustering. Recently, contactin-associated protein (Caspr), a 180-190-kD neuronal glycoprotein that is a potential cell adhesion molecule, was identified and shown to accumulate in the paranodal axolemma (Peles et al., 1997; Einheber et al., 1997). Furthermore, during development, Caspr is first uniformly expressed on the surface of axons and later, as myelination proceeds, its distribution becomes restricted to the paranodal regions (Rasband et al., 1999a). This is the first event in the axonal domain formation, followed by the cluster formation of the ion channels, suggesting that paranodal junctions play a crucial role in the organization of the nodal regions. K^+ channels are diffusely localized in the CNS axons of hypomyelinating *shiverer* mutant mice (Wang

et al., 1995), and their clustering also disappears after demyelination by intraneural injection of lysolecthin in the peripheral nerve (Rasband et al., 1998). Thus, the role of myelin or myelin-forming glias on the distributional change of the axonal proteins may be different between the clustering of Na^+ and K^+ channels.

In addition to ion channels and Caspr, other specific molecular markers in each axonal domain have been identified recently. $Ankyrin_G$ (Srinivasan et al., 1988; Lambert et al., 1997; Bennett et al., 1999) and certain cell adhesion molecules (neurofascin 186 and NrCAM) form complexes with Na^+ channels at the nodes, whereas Caspr2 is associated with K^+ channels at the juxtaparanodes (Fig. 1, Davis et al., 1996; Poliak et al., 1999). Besides, Caspr and its binding partner, contactin, are highly concentrated at the paranodal junctions and may physically separate the Na^+ and K^+ channels by inhibiting lateral movement of these proteins (Fig. 1, Boyle et al., 2001, Bhat et al., 2001). These axonal proteins are useful as specific markers to each domain. Up to now most of the major myelin proteins in both CNS and PNS have been identified and their genes have been cloned already. Studies on spontaneous myelin mutants as well as gene-manipulated mice showed that some of these mice lack a specific portion of myelin such as compact myelin and paranodal junction, and they allow us to investigate a role of specific part of myelin in directing the axonal domain formation. In this chapter, I investigated the domain organization using specific antibodies against Na^+ and K^+ channels and Caspr in various mutant and gene-manipulated mice as well as myelinated and unmyelinated regions in adult and developing normal mice. Using these mice, I studied axonal protein localization in hypomyelinated, paranodal abnormal or demyelinated mice.

Results

Domain organization in myelinated and nonmyelinated axons

First, to clarify whether the myelin membrane itself can induce the distributional change of axonal ion channels, I investigated the axonal domain organization in adult mouse optic nerve. Axons from retinal ganglion cells (RGC) consist of clearly demarcated unmyelinated and myelinated regions within a single axon. In most mammals oligodendrocytes are excluded from the retina, therefore RGC axons remain unmyelinated until they exit from the eye ball at the lamina cribrosa. After passing the lamina cribrosa and entering into the optic nerve, the RGC axons become myelinated. Thus the optic nerve is an ideal place to study the role of myelin sheaths on the expression and localization of ion channels by comparing unmyelinated and myelinated regions within the same axon. The transition from the unmyelinated to myelinated regions was clearly demonstrated by immunostaining using myelin protein antibodies (Fig. 2, Baba et al., 1999). Figure 2a shows a section through the adult mouse optic nerve immunostained with antibodies against neurofilament (NF) as a marker of axon and against a major myelin protein, myelin basic protein (MBP). To examine localization of Na^+ and K^+ channels in these two regions, double immunostaining was performed using anti-Na^+ channel (green) and Kv1.1 potassium channel α subunit (red) antibodies. Immunoreactivities of both channels were distributed uniformly along the unmyelinated portion of RGC axons (Fig. 2b). In contrast, distinct cluster formation of both channels was observed in the myelinated region (Fig. 2c) in the same nerve. Localization of other K^+ channel α subunits Kv1.2 and Kvβ2 β subunit showed a similar pattern to that of Kv1.1 (data

not shown). Normally, the node of Ranvier is delineated by Caspr, which is an axonal membrane protein localized at the paranodal region of myelinated axons (Peles et la., 1997). Figures 2d and e show Caspr (green) and Kv1.1 (red) immunoreactivities in the unmyelinated and myelinated regions of the RGC axons. In the unmyelinated region, the immunoreactivity of Caspr was strong but diffuse (Fig. 2d), whereas in the myelinated region this immunoreactivity clearly formed clusters adjacent to the K^+ channel clusters (red) (Fig. 2e). In addition, such Caspr immunoreactivity never overlapped with Na^+ channel immunoreactivity. These findings were consistent with the previous proposal that myelin membranes or oligodendrocytes are necessary for clustering of ion channels as well as Caspr in adult mouse axons (Baba et al., 1999, Rasband et al., 1999a).

In developing axons

The myelination process includes several steps, such as migration and maturation of oligodendrocytes, ensheathment of axons with their processes, and compaction of myelin sheaths. At the final stage of myelination, the paranodal loops of myelin make contact with axons and form a tight seal around them (Rosenbluth, 1995b). To know the involvement of myelin on the axonal domain organization in more detail, I examined the localization of these proteins during myelianation. Previously myelination in the developing mouse optic nerve was examined using electron microscopy (Fig. 3g, Baba et al., 1999). Diamond shapes (◆) in Figure 3g indicate the percentage of axons covered by compact myelin. The myelin sheaths appeared around postnatal day 8 (P8), and that the number of myelinated fibers began to increase at P10, although most of myelin sheaths at this age were still thin and

uncompacted. At P14, the number of myelinated axons dramatically increased and the compaction of myelin sheaths started, but more than 70% of axons were still naked at this time. Thereafter the number of myelinated axons steadily increased, and by one month of age, more than 70% of the axons were finally covered by compact myelin sheaths. The thickness of the compact myelin also increased gradually during this period.

I examined the timing of Na^+ and K^+ channels cluster formation during the development of mouse optic nerves every other day from P7 to P28. It was revealed that Na^+ and K^+ channels did not form clusters until P9. Na^+ channel clusters were first detected at P9-P10 although the number of clusters was fewer than 5 per fields of view (FOV; 1 FOV= $73.1 \times 73.1\ \mu m^2$) (n=10, Fig. 3a). During the third week of age, from P15 to P19, the number of Na^+ channel clusters increased dramatically from an average of 13 (P15) to 38 (P19) per FOV (n=10, Fig. 3b, c, d). During this immature period, the length of the clusters tended to be longer in comparison to those observed at the mature stages (Fig. 3a asterisk) and a small number of binary-shaped (Fig. 3d asterisk) Na^+ channel clusters were observed transiently (11% at P15, decreasing to 3% at P19). Then at P28 (Fig. 3f), the number of Na^+ channel clusters was nearly equivalent to that observed in adulthood (8-week-old of age) (54 ± 2 and 61 ± 1 clusters per FOV, respectively). After that, as myeliantion proceeded, the Na^+ channel were condensed into focal clusters (compare Fig. 3a to Fig. 3f).

In contrast, K^+ channel clusters were not found until P14. Between P15 to P17, K^+ channel clustering began to be detected near the Na^+ channel clusters, and most of these clusters already appeared as a paired punctate pattern (Fig. 3c, d). However, only about 60% of the K^+ channel clusters in the adult (8-week-old) were observed at

P28, by the time when the Na^+ channel clusters were already detected almost as many as in adult mice (Fig. 3f). The number of juxtaparanodal K^+ channel clusters continued to increase during the development until all the K^+ channel clusters became associated with the Na^+ channel clusters. The relationships between the myelination process and ion channel clustering were plotted in Figure 3g. The timing between the appearance of Na^+ channel clustering and K^+ channel clustering were observed to be distinct from each other. From this developmental study, I found that Na^+ channel forms clusters simultaneously or slightly before the appearance of compact myelin on the axon, and that K^+ channel forms clusters only after myelin compaction is completed. These results suggest that early steps of myelination are required for Na^+ channel clustering, whereas later steps are crucial for the initiation of K^+ channel clustering.

Under hypomyelinated condition

To clarify the role of the myelin membranes in the formation of ion channel clusters on myelinated axons, the changes of axonal domains in the hypomyelinating mutant mice *jimpy*, which contain a point mutation in the myelin proteolipid protein (PLP) gene, were examined (Nave et al., 1987). In the *jimpy* CNS, the number of mature oligodendrocytes is reduced by ~50% (Knapp and Skoff, 1987) due to an extensive premature oligodendroglial cell death; thus only 1-3% of *jimpy* axons are surrounded by myelin sheaths compared with those of normal littermates (Duncan et al., 1989). I used optic nerves from P21 *jimpy* mutants and their littermate controls to examine Na^+ and K^+ channel clustering under the hypomyelinated condition. Interestingly, although only a small numbers of axons were surrounded by myelin membranes, the

number of Na^+ channel clusters observed in this mutant (Fig. 4d-f) was retained to approximately 65-75% of that in littermate controls (Fig. 4a-c). At P21, a few broad clusters remained even in the optic nerve from wild-type mice (Fig. 4b asterisk), although most of the Na^+ channel clusters became focal in shape (Fig. 4c). In contrast, relatively few Na^+ channel clusters were focal shapes (<1.2μm) in the mutant, and more than 70% (92 out of 132 clusters from three animals) of these clusters displayed irregular dot-like, broad (Fig. 4e) and binary (Fig. 4f, asterisk) shapes at all the optic nerve regions from the lamina cribrosa to chiasma. Thus only 20 % of the clusters in the mutants appeared normal in comparison to the wild type control. Double labeling of the *jimpy* optic nerve using anti-Na^+ channel (green) and anti-MBP (red) antibodies revealed that the sites of Na^+ channel immunoreactivity were not always related to the MBP positive signals (Fig. 5b).

As described in Fig. 3g, K^+ channels clusters first appeared approximately 2 weeks after birth, and at P21 some, but not all of the clusters, were observed in the juxtaparanodal regions of the optic nerve from littermate controls (Fig. 4a-c). From double-immunostaining using anti-MBP and anti-Kv1.1 antibodies, MBP staining in the wild type controls showed that the axons were already covered with myelin membrane and that K^+ channels formed clusters at the juxtaparanodal regions (Fig. 5c), whereas these channels were distributed diffusely in *jimpy* optic nerves (Fig. 4d-f). Occasionally, some K^+ channel-positive clusters were observed near the MBP staining (Fig. 5d).

Jimpy optic nerve sections were also double-stained with anti-Na^+ channel and anti-Caspr antibodies. If Na^+ channel clustering in the optic nerve is mediated by direct interaction with myelinating oligodendrocytes, some Caspr clusters should be

detected next to such Na^+ channel clusters. If, in contrast, the clustering of Na^+ channels is independent of the glial process, Caspr clusters may not be observed at all in the mutant optic nerve. In littermate controls, nodal Na^+ channel clusters (red) were sharply demarcated by a pair of Caspr clusters in the paranode (Fig. 6a). In contrast, such Caspr (green) clusters were never observed, even in an irregular form, and were diffusely distributed throughout the axolemma in the optic nerve from *jimpy* mutants (Fig. 6b). In addition, I examined the distribution of the cytoskeleton-associated molecule $ankyrin_G$, which has been shown to bind to Na^+ channels *in vitro* (Srinivasan et al., 1988) and is localized at the nodes of Ranvier (Kordeli et al., 1995). $Ankyrin_G$ immunostaining in the control littermate optic nerve (Fig. 7a, d, red) colocalized exactly with Na^+ channels (green) as intensely labeled nodal regions. Additionally, weaker immunofluorescence was also observed in the paranodal regions (Fig. 7a, arrow), which may be due to cross reactivity with other members of the ankyrin family (Lambert, by personal communication). In the *jimpy* mutant, the aggregation of $ankyrin_G$ was irregular and always colocalized with Na^+ channels (Fig. 7b, d, e). These observations suggest that while the paranodal loops and compact myelin may not be necessary for the initial clustering of Na^+ channels at the node of Ranvier, the paranodal loops may be required for the formation of the properly shaped clusters. Myelin is essential for clustering of K^+ channels on the axons. These results are consist with the observation made in the *jimpy* corpus callosum (Mathis et al., 2001) and with the recent results obtained by Jenkins and Bennett (2002).

Axonal domain organization under abnormal paranodal condition

Myelin is morphologically classified into two regions, compact myelin and paranodal

loops (Fig. 1). The paranodal myelin loops form septate-like junction with paranodal axolemma (for review Tepass et al., 2001). This junctions is believed to work as a diffusion barrier for Na^+ and K^+ channels, and the cells on both sides may communicate each other through this region. To clarify the role of the paranodal loops on axonal domain formation, I analyzed the distribution of axonal proteins in the galactosylceramide sulfotransferase (CST)-deficient mice (Honke et al., in press). These mice are incapable of synthesizing one of the major glycolipids, sulfatide, through disruption of the CST gene. These mice are born normal and survive over one year of age, but develop neurological deficits such as hindlimb weakness and tremor after 6 weeks of life. From electron microscopic studies, these mice exhibited paranodal abnormalities such as terminal loops facing away from the axons (Fig. 8a, b, Honke et al., submitted) but the compact myelin is intact (see the results below). Thus, the CST-deficient mice provide us with valuable informations to understand the role of the paranodal loops on the establishment of axonal domains separately from those of compact myelin membranes.

First, I examined the myelin structure by immunohistological and biochemical studies of MBP and PLP/DM20. No apparent changes were observed in the staining pattern of a major myelin protein, MBP, between the mutant and control optic nerves at 22 weeks of age (Fig. 8c, d). The PLP/DM20 staining of the optic nerves also revealed no significant changes (data not shown). Furthermore, each protein level in the CNS myelin fraction was examined by Western blot analysis. As shown in Fig. 8e and 8f, the intensities of the specific bands of MBP (e) and PLP/DM20 (f) were unaltered between the mutants and the controls. Thus, no significant changes of major myelin proteins were detectable by immunohistochemical as well as Western

blot analysis. These results were confirmed by electron microscopical study by Dr. Dupree. The electron microscopical analysis of the optic nerve cross sections of 29-week-old wild type (Fig. 8g) and CST-deficient (Fig. 8h) mice revealed no morphological difference in compact myelin between the two. Taken together, these results demonstrated that the CST-deficient mice exhibit only paranodal disruption of myelin membranes. I then analyzed the distribution of the voltage-gated Na^+ and K^+ channels in CNS (optic nerve and spinal cord) sections from adult (14w) CST-deficient mice. In contrast to wild type control (Fig. 9a), the localization and cluster shape of both ion channels were altered in the spinal cord (Fig. 9b-d) and optic nerves (Fig. 9e-h) of the CST-deficient mice. In the mutant mice, Na^+ channels formed clusters in the presumptive nodes, however, the lengths of these clusters were occasionally longer than those in the wild type (Fig. 9, compare a and b, f). I measured the lengths of Na^+ channel clusters, which were indicated by the fluorescence intensity in the optic nerves. In 16-week-old littermate controls, the cluster lengths were nearly constant (0.79 $\pm$ 0.05 μm; more than 100 nodes were examined from two mice). In contrast, in the CST-deficient mice, the Na^+ channel immunoreactivity became significantly longer in comparison to those of the control mice (1.25 $\pm$ 0.05 μm; more than 75 nodes were examined in each of two mice; $P < 0.001$ by t test) (Fig. 9i). In addition, the binary appearance of Na^+ channel clusters was frequently observed in the mutant mice (Fig. 9d, h). In the optic nerves from 10-week-old mutant mice, 11% (25 out of 236 clusters from two animals) of the Na^+ channel clusters were binary shaped, and 12% (31 out of 245 clusters from two animals) in the 14-week-old mice. Such binary-shaped clusters appeared occasionally in a relatively early stage of normal development, but were never observed at this age.

K^+ channel distribution in the CST-deficient mice was more severely affected than Na^+ channel distribution. Although the K^+ channel antibody occasionally stained the paranodal regions even in the wild type mice, the intensity of the paranodal staining was significantly weaker than that of the juxtaparanodal clusters (Fig. 9a). In the mutant mice, in contrast, the K^+ channel clusters frequently accumulated aberrantly in the regions adjacent to the Na^+ channel clusters, presumptive paranodal regions, in addition to the juxtaparanodal regions (Fig. 9b, c, d, f). As shown in Figure 9c and f, the intensities of the K^+ channel staining in some of the presumptive paranodes were even brighter than those in the juxtaparanodal regions. Heminodal formation that labeled just one side of the juxtaparanode or presumptive paranode with the antibody against Kv1.1 was also observed in the mutant mice (Fig. 9g). The staining patterns observed using antibodies against other K^+ channel subunits, Kv1.2 and Kvβ2, were similar results (data not shown). These data suggested that the paranodal axo-glial junction regulate proper localization of ion channels, however, it is not essential for the cluster formation itself.

I also analyzed the distribution of Caspr. Double-labeling with Caspr and K^+ channel antibodies revealed paired patterns of these proteins next to the unlabeled node in wild type optic nerve (Fig. 10a). On the contrary, this type of paired staining was absent in the CST-deficient mice, and Caspr appeared to be diffusely distributed along the axons as shown in Figure 10b, c (optic nerve). In 6-week-old mice, although a small number of Caspr clusters were observed adjacent to some of the K^+ channel clusters, most of the channel clusters were not associated with Caspr (Fig. 10b). In 10-week-old mice, Caspr clusters were hardly recognized and a diffuse staining pattern was observed throughout the axons in the CST-deficient mice (Fig. 10c). Such

diffuse distribution of Caspr was also observed in hypomyelinating axons as well as in unmyelinated fibers, suggesting that the aggregation of Caspr could be induced only in the presence of paranodal junction as previously described (Rasband et al., 1999a).

To understand better whether the myelin paranodal loops have some influence on the establishment of axonal domain specification, I analyzed the localization of Caspr and Na^+ channel clusters carefully during development in CST-deficient mice (Fig. 10b, c, e) and in wild type littermate (Fig. 10a, d). No significant changes were observed in the number of Na^+ channel clusters between mutant and wild type mice (23 ± 4 clusters per FOV in littermate control, 21 ± 2 clusters per FOV in the mutant mice; n=12 from two animals each). In contrast, no Caspr clusters were observed in CST-deficient mice at P17 (Fig. 10e). Western blot analysis of brain revealed no differences in the protein levels between the mutant and wild type mice (Fig. 10f), indicating that the diminished immunoreactivity of Caspr is, in fact, a result of dispersed distribution of this protein throughout the entire internodes.

Chronic demyelination

Several previous studies based on electrophysiological and immunohistochemical experiments suggested that axonal ion channel localization was affected by removal of myelin sheath in the PNS axons (Richie et al., 1981; Rasband et al., 1998). Although the main devastation occurred in myelin sheaths in either study, some extent of axonal damage could not be excluded under the demyelinating conditions used. In the transgenic mice containing extra copies of the PLP gene (PLP *tg* heterozygotes) (Kagawa et al., 1994), the myelin sheaths are formed normally during development, but demyelination starts around 5 months of age (Inoue et al., 1996). Such

demyelination progresses rapidly, and most of the axons finally become completely naked by 7 months of age. The demyelination in these mice is not accompanied by secondary inflammation or axonal degeneration. Therefore, this is an ideal animal model to examine whether the CNS myelin membrane is required for the maintenance of axonal domains which had been established during development. To verify the localization of the Na^+ and K^+ channel accumulation, I double-labeled the optic nerve from 9-week to 13-month-old heterozygotes and wild-type littermates with antibodies directed against Na^+ and K^+ channels (Fig. 11). At 9 weeks of age, when no demyelination had occurred yet, characteristic channel distribution was observed in heterozygote mice (Fig. 11a). At 5.5 months of age (Fig. 11b, c) the number of Na^+ channel clusters were still maintained, even though this number was less than that observed in 9-week-old mice. As demyelination progressed, the number of Na^+ channel clusters decreased gradually with age. The average numbers of Na^+ channel clusters decreased from 48 per FOV (n=9) in 7-month-old (Fig. 11d, j) to 27 (n=9) in 10.5-month old PLP *tg* (Fig. 11e, j). At 13 months of age (Fig. 11f, j), these clusters were markedly decreased and only 13 clusters per FOV remained. Furthermore, various irregular forms of sodium channel clusters such as an elongated broad form (>1.2μm) or a binary form were frequently observed during demyelination (Fig. 11g, h). These cluster types were never observed in wild type mice of the same age.

K^+ channels were concentrated at the juxtaparanodes of wild-type as well as heterozygote mice at 9 weeks of age (Fig. 11a, j). By 5.5 months of age (Fig. 11b, c, j), the accumulations of K^+ channel in the juxtaparanode decreased dramatically from average of 56 to 29 clusters per field of view (FOV; 1 FOV=73.1 x 73.1 μm^2, n=9), and these numbers kept decreasing rapidly with age. Only 19 or 7 clusters per FOV (n=9)

were detected at 7 or 10.5 months of age, respectively (Fig. 11d, e, j). Eventually, all of K^+ channel clusters disappeared in the 13-month-old optic nerve of the heterozygote (Fig. 11f, j). The same reduction rate was obtained when other α subunit Kv1.2 and β subunit Kvβ2 antibodies were used (data not shown). These data using PLP *tg* heterozyotes indicated that myelin sheaths (compact myelin and paranodal loop) are required for the maintenance of clustering of Na^+ and K^+ channels, although the involvement of the myelin on their maintenance is different between the two channels. To determine whether K^+ channel reduced its protein level in demyelinated axons or it redistributed diffusely, the protein level of each subunit in demyelinating optic nerves was examined by Western blot analysis. Fig.11i showed that both K^+ channel subunits, Kv1.1 and Kvβ2, were not reduced at the protein level after demyelination, suggesting that the disappearance of the clusters was due to the redistribution of K^+ channels.

Discussion

In this chapter, I analyzed the axonal domain organization using specific antibodies against Na^+ channels, K^+ channels, and Caspr under several conditions to understand the role of myelin: unmyelinated and myelinated axons, development, hypomyelination, paranodal abnormality, and demyelination. The change of channel clusters on the axons under each myelin condition is summarized in Table 1. For axonal voltage-gated Na^+ channels and K^+ channels, it turned out that requirement of myelin or myelin-forming cells was in a distinct manner, respectively. I discuss current evidence about possible myelin function on Na^+ and K^+ channel clustering.

Clustering of nodal voltage-gated Na^+ channels in myelinated axons

There is evidence from both electrical and immunocytochemical experiments that the gradient of Na^+ channel density at the node is very sharp in the myelinated axons (Shrager, 1989; Dugandzija-Novakovic et al., 1995). What mechanisms are responsible for the clustering of Na^+ channels? Currently, three hypotheses have been presented. First, Na^+ channels form clusters under neuronal control and it can occur independently from myelination. Second, a humoral factor from myelin-forming glial cells induces the clustering. The third model asserts that clustering requires direct contact of myelinating glial cells (Salzer, 1997). Although it is still controversial, the present study using mice in normal and pathological conditions gave some new insights into this issue.

The study of adult optic nerve clearly indicated that the Na^+ channel clusters were formed restrictly in the myelinated axons but never in the unmyelinated axons

(Fig. 2, Table 1). Because the axon needs to sense the presence of glial signals to specify the nodes, the first hypothesis can be ruled out, and it can be conclude that either myelin sheaths or oligodendrocytes are essential for initial clustering of the Na^+ channels. Then, the next question to be solved is whether myelin itself is responsible for initial channel clustering. In the myelinated optic nerve, the initiation of axo-glial adhesion assembly is a very early event, since paranodal junctions can be detected as soon as the first spiral of the oligodendrocyte process ensheathes an axon (Wiggins et al., 1988). Hence, I determined the formation of the axo-glial junction using Caspr immunoreactivity and examined whether Na^+ channel clusters appear before or after the junctional formation. As summarized in Table 1, Na^+ channels can form clusters even when no Caspr clusters appear during development of normal, CST-deficient, and hypomyelinating *jimpy* mutant mice. In *jimpy* mutant, many Na^+ channel clusters were observed even where no MBP positive myelin sheaths were detected. The same results were obtained using another nodal marker $ankyrin_G$. This $ankyrin_G$ is also a nodal protein and an attractive candidate to mediate the clustering of Na^+ channels (Kordeli et al., 1995; Zhou et al., 1998) probably by forming heterocomplexes with Na^+ channel and NF186 in vivo (Michaely et al., 1995; Zhang et al., 1998). During development, around P7, appearance of $ankyrin_G$ immunoreactivity preceded that of Na^+ channel (appearing first in the paranodal region and later extending through the nodal gap; data not shown; also Rasband et al., 1999a). In *jimpy* mutant, Na^+ channel and $ankyrin_G$ always colocalized (Fig. 7), suggesting that the places where Na^+ channel formed clusters in this mutant actually had nodal characters. Thus, neither compact myelin nor early paranodal axo-glial junction is essential for initial clustering of Na^+ channel. Then, it remains controversial whether direct glial contact is required for

initial determination or humoral factor is sufficient.

Rasband et al. (1999a) reported that Caspr immunoreactivity was found at the edge of myelin-associated glycoprotein (MAG)-labeled processes at P7, but Na^+ channel clusters were not seen until P9-10. Further, they examined other hypomyelinating mutant mouse, *shiverer*, which has a deletion in the MBP gene, resulting in loss of compact myelin in the CNS (Rosenbluth, 1980; Inoue et al., 1981). Although only a small number of Na^+ channel clusters were present in this mutant, these clusters were always adjacent to the Caspr clusters. From these results, they concluded that Na^+ channel clustering at the nodes depends on axo-glial contact which is indicated by Caspr immunoreactivity. They also described that 12% of the Na^+ channels had only weak or undetectable level of neighbouring Caspr immunofluorescence during development, however, most of their observations were totally inconsistent with ours. It may be necessary to find another marker for axo-glial contact, since the initial contact required for the nodal determination can not be detected by Caspr immunoreactivity.

Kaplan et al. (1997) reported that a protein secreted by oligodendrocytes induced Na^+ channel clustering at a regular intervals corresponding to future internodal distance without any attachment of myelin in the cultural CNS neurons. There is a report of *myelin deficient* (*md*) rat, which is characterized by a defect in the PLP gene and resulting hypomyelination in the CNS (Dentinger et al., 1982). By freeze-fracture replicas of *md* rat spinal cord axons, focal patches of particles were found in the area corresponding to the partial node-like structures seen in thin sections (Rosenbluth, 1995b). Scherer's laboratory (Brophy, 2001) showed that Na^+ channels formed clusters in the CNS axons of *md* rats. Recently Mathis et al. (2001) and Arroyo et al.

(2002) reported the presence of the Na^+ channel clusters in the *jimpy* mice and *md* rats, respectively. Further, ultrastructural studies indicated that the axon begins to differentiate and displays foci of membranes with nodal properties even before the onset of myelination (Waxman and Black, 1995). Although these findings may suggest that a soluble factor can cause Na^+ channel clustering, it is still possible that there is some direct contact of oligodendrocyte processes. Further, since there is no apparent barrier between unmyelinated and myelinated regions, it is hard to imagine that such a humoral factor works locally in the myelinated area of the optic nerve. My result showing that the clear distinction exists between myelinated and unmyelinated is supporting the later direct contacts hypothesis.

Another possibility is that perinodal astrocyte (Sims et al., 1985) plays an instructive role in Na^+ channel clustering, since radial processes of astrocytes are always colocalized with the patches of node-like membrane in normal and *md* rat axons (Rosenbluth, 1995a, Waxman and Black, 1995). Gap junctions are also present between perinodal astrocytes and oligodendrocytes surrounding the node of Ranvier. Furthermore, a chondroitin sulfate proteoglycan NG2 positive process from immature oligodendrocyte is found in the nodal region recently (Martin et al., 2001). It is possible that initial trigger of Na^+ channel clustering is regulated by contact with either cell types, and that the channel aggregation may be then accelerated by paranodal direct contacts between axons and myelin membranes.

Then, how the paranodal axo-glial junction and the compact myelin have influence on the nodal formation? The significant morphological variances such as elongated (> 1.2 μm) and binary shaped clusters were observed (Fig. 3a, d) during the period of Na^+ channel cluster formation (P9-P19, Fig. 3g), and these were never

detected in the adulthood. Such observation is consistent with the previous report using rat optic nerve (Rasband et al., 1999a). Furthermore, they calculated conduction velocities in the developing optic nerve, and concluded that significant functional changes were accompanied by both the number and the average length of the clusters. Therefore, the staining pattern of anti-Na^+ channel antibody reflects the process of nodal maturation, so an immature node can be recognized as a broad or binary cluster (> 1.2 μm) of Na^+ channel, and a mature node as a focal cluster (< 1.2 μm). Interestingly, when myelin had some abnormalities such as hypomyelination (Fig. 7e-f and Table 1) or paranodal disruption (Fig. 9b-h and Table 1), Na^+ channel clusters were always detected as the same immature shapes in normal development. Moreover, in spite of the presence of Na^+ channel at the node, these mutants developed remarkable neurological phenotypes. Thus, both compact myelin and paranodal junction are required for the nodal maturation, which is essential for the establishment of rapid nerve impulse conduction during development.

Clustering of juxtaparanodal voltage-gated K^+ channels in myelinated axons

K^+ channels are clustered beneath the myelin sheath at juxtaparanodes (Fig. 1). I studied which myelination processes are responsible for K^+ channel clustering at the juxtaparanode. The present study showed that late steps of myelination are crucial for the initiation of K^+ channel clustering at the juxtaparanode (Fig. 3g). The presence of myelin or oligodendrocyte cell bodies is not sufficient for K^+ channel clustering, but myelin compaction and probably the formation of axo-glial junction are required for the initiation of K^+ channel clusters at the juxtaparanode. These findings are consistent with the previous developmental studies (Baba et al., 1999; Rasband et al.,

1999b). This requirement of compact myelin and/or paranodal loops was also confirmed by the experiments in *jimpy* mouse (Fig. 4-6). Furthermore, the study on CST-deficient mice provided additional information about the formation of K^+ channel clusters. The CST-deficient mice exhibited disruption of paranodal junction, and in this animal K^+ channel clusters were formed but mislocalized to the presumptive paranode (Fig. 9). A similar phenomenon was observed in other mice displaying paranodal disruption, in which K^+ channel clustering was aberrantly localized (Dupree et al., 1999; Poliak et al., 2001; Bhat et al., 2001; Boyle et al., 2001). These results clearly demonstrated that compact myelin is essential for initial clustering of K^+ channel, but the paranodal junction is not absolutely required for this process. In contrast, the proper localization of K^+ channel clusters requires both axo-glial junction and compact myelin, because the K^+ channel clusters change their localization to presumptive paranodes instead of internodes under abnormal paranodal conditions. Whenever the position of K^+ channel clusters was mislocalized, they were always directly adjacent to (Fig. 9c, d, f) or very close to (Fig. 9g) Na^+ channel clusters, as if K^+ channel clusters tend to be attracted to the Na^+ channel clusters. It is possible that K^+ channel clusters are not directly anchored to the axonal cytoskeleton but are accumulated in the juxtaparanodal region by unknown attractive force from the nodal region.

The mechanism underlying the cluster formation of K^+ channel is also not known and may involve their association with other axonal molecules including Caspr2. Caspr2 is the second member of the Caspr family and is more closely related to *Drosophila* neurexin IV than to Caspr. Under abnormal paranodal conditions, the localization of Caspr2 also moves to the paranodal region associated with K^+ channel

clusters (Poliak et al., 2001). Reciprocal co-immunoprecipitation experiments suggested that indirect interaction between the Kv1.1, Kv1.2 and Kvβ2 β subunits, and Caspr2, probably through a PDZ-domain-containing protein (Poliak et al., 1999). One candidate for this PDZ-domain-containing protein is postsynaptic density protein-95 (PSD-95) or its related protein (Sheng and Kim, 1996), which is known to bind directly to the carboxyl-terminal cytoplasmic tail of shaker-type K^+ channel (Kim et al., 1995). The presence of PSD-95-like protein in the juxtaparanode along with K^+ channel was recently demonstrated (Baba et al., 1999), and in CST-deficient mice, localization of the PSD-95-like protein also moved to the presumptive paranode with K^+ channel clusters (data not shown). Therefore, although crucial function of these proteins at the juxtaparanode is yet uncertain, these molecules may play certain roles in the formation of K^+ channel clusters.

Present studies also indicated that myelin is required for the maintenance of the axonal domains in the CNS, even after they have been once established during development. The study using PLP *tg* heterozygotes showed that K^+ channel localization immediately changes when demyelination occurred (Fig. 11j, also in Baba et al., 1999). Thus, K^+ channels require compact myelin constantly, not only for the initiation, but also for the maintenance of their characteristic cluster. This finding also supports the hypothesis described above that K^+ channel clusters are not directly anchored to the cytoskelton, so that they can be easily disrupted. Na^+ channel clusters, on the other hand, were maintained relatively longer even in the absence of myelin sheaths, but eventually most of the clusters disappeared (Fig. 11f, j). This difference in the timing of disappearance of the clusters between the Na^+ and K^+ channels may result in conduction block, which is commonly observed in demyelinating diseases.

Chapter II

Introduction

What kinds of myelin components are involved in axonal domain formation?

Paranodal axo-glial junctions flank the node of Ranvier in myelinated nerves. The results reported thus far including our findings suggested that although neither Na^+ nor K^+ channels are present in the paranodal region, the axo-glial paranodal junction is essential for the proper localization of both Na^+ and K^+ channels around the node of Ranvier. Furthermore the neurological defects are caused by disruption of the paranodal junction, suggesting that the integrity of the junction is also crucial for nerve conduction. Molecular organization of myelin loops as well as axolemma at the paranode has recently come to light. So far, three proteins have been identified as specific components of the paranodal complex. The axonal membrane at the paranode contains Caspr and glycosylphosphatidylinositol (GPI)-anchored cell adhesion molecule, contactin (F3/F11) (Berglund and Ranscht, 1994). The direct interaction between Caspr and contactin are required for the cell-surface expression of Caspr (Faivre-Sarrailh et al., 2000). The glial membrane at the paranode conains neurofascin 155 (NF155), an ankyrin binding member of the L1 family, which was identified as the first glial molecule (Tait et al., 2000). Although NF155 is a candidate counterpart of Caspr or contactin in the paranodal loops, whether this glial cell adhesion molecule interacts with these axonal proteins is yet to be determined. Recent immunoprecipitation study between NF155 and Caspr suggests that there may be other additional molecules involved in the paranodal formation.

Previously two research groups (Bosio et al., 1996; Coetzee et al., 1996)

generated mice with a disruption of the gene that encodes UDP-galactose: ceramide galactosyltransferase (CGT), the enzyme that catalyzes an essential step in the biosynthetic pathway of two myelin glycolipids, galactocerebroside (GalC) (Morell and Radin, 1969) and its sulfated derivative (sulfatide). These mice displayed some nodal and paranodal abnormalities, including altered nodal lengths, heminodes, absence of the transverse bands, and the presence of reversed lateral loops (Coetzee et al., 1996). Immunohistochemical studies showed abnormal distributions of K^+ channels and Caspr in the myelinated axons (Dupree et al., 1999). However, since this mutant lacked two major glycolipids in addition to unusually accumulated hydroxy fatty acid (HFA)-glucocerebroside and HFA-sphingomyelin in the myelin, it was impossible to identify independent function of these two lipids, GalC and sulfatide, in the paranodal junction. As described in Chapter I, the mice incapable of synthesizing sulfatide but not GalC through disruption of the galactosylceramide 3-sulfotransferase (CST) gene have been generated (Honke et al., in press). Since these mice exhibited paranodal abnormalities as revealed by electron microscopical studies (Chapter I, Fig 8), I analyzed the distribution of the axonal proteins in CNS of the CST-deficient mice. As expected, all the abnormalities of channel distributions reported in the CGT-deficient mice (Dupree et al., 1999) were also observed in the CST-deficient mice (Chapter I, Fig. 9). Thus, sulfatide itself is one of the essential myelin components to induce the formation of the paranodal junction as well as the axonal domains, at least in CNS.

From the structural characteristics, the paranodal junction is thought to be formed through binding of adhesion molecules from both axonal and glial sides, and those are probably anchored by proteins connecting to cytoskelton. Previous studies

demonstrated that glycosphingolipids select certain proteins for subcellular transport via detergent-insoluble glycolipid-enriched complexes (DIGs) (Ledesma et al., 1998). Therefore the role of myelin sulfatide seems to mediate axo-glial junction indirectly by regulating intracellular protein trafficking in myelin forming cells, and such unidentified glial proteins may be sufficient to direct both Caspr and contactin to the paranode. To search other myelin molecules involved in this junctional formation, I examined the distribution of axonal proteins in several mutant mice, each of which lacks an individual myelin component. As a result, I found that one candidate molecule, CD9, is participating in paranodal formation.

CD9 is a 24-27 kDa cell surface glycoprotein (Boucheix and Benoit, 1988) expressed in a wide variety of cells and is a member of the tetra-membrane-spanning protein (TM4)/the transmembrane-4 superfamily (TM4SF). A number of studies have suggested that CD9 plays some roles on cell signaling, cell adhesion, cell motility, and tumor cell metastasis (for review by Maecker et al., 1997). CD9, which can associate with integrins such as $\alpha 3\beta 1$ or $\alpha 6\beta 1$, is a possible co-factor of the integrins (Nakamura et al., 1995). In the PNS, CD9 regulates Schwann cell motility that is correlated with a rise in cytosolic calcium level and subsequent tyrosine phosphorylation *in vitro* (Anton et al., 1995). In the CNS, Schmidt et al. (1996) showed CD9 expression in several kinds of cells *in vitro*, and demonstrated that an anti-CD9 antibody (H6) promotes neurite outgrowth and cell migration associated with $\alpha 6\beta 1$ integrin and neural adhesion molecule L1. Furthermore, since this protein appears at the final stage of myelination (Kagawa et al., 1997) and is localized along the outermost membrane of myelin (Nakamura et al., 1996), it is a good candidate that is involved in the paranodal formation. To identify the functional role of CD9 in the process of the

paranodal formation, I analyzed the detailed localization of this protein and alteration of axonal domains in mice lacking CD9. In this Chapter II, I focused on the functions of two molecules, CD9 and sulfatide, for the paranodal as well as axonal domain formation both in the CNS and PNS.

Results

CD9 is localized in the paranodal axo-glial juction as well as outermost membrane of myelin

I analyzed the localization of CD9 in the CNS and PNS using normal adult C57BL mice. The sections were double-labeled with antibodies against CD9 and Caspr (Fig. 1a-c). Although the distributions of CD9 (green) and Caspr (red) overlapped slightly (yellow, b, c arrow), paranodal localization of CD9 was difficult to detect. In the PNS, in contrast, the immunoreactivity of CD9 indicated that this protein formed a pair of clusters in addition to the diffuse distribution in the outermost membrane of myelin (Fig. 1d). Such characteristic CD9 clusters were proved to be located in the paranodal regions of sciatic nerve because of colocalization with Caspr (Fig. 1e). To understand the functional role of CD9 in the process of paranodal formation, I investigated the detailed localization of this protein during PNS development using teased fibers. At P0 and P1, prior to myelin ensheathment, CD9 was first observed in the cell body of the Schwann cells (Fig. 2a, b arrow). At P2, when some axons began to myelinate, CD9 became concentrated in the bilateral ends of myelin (Fig. 2c arrow) as well as myelin surface. By P4, Schwann cells begin myelination, and CD9 become progressively accumulated at the presumptive paranode (Fig. 2d). These results suggest that CD9 is one of the important myelin components for the formation of paranodal junctions in the PNS.

CD9-deficient mice display paranodal abnormality

The localization of CD9 at the paranodal regions raised the question if the lack of CD9

expression may affect the axo-glial paranodal junctions. To address this issue, I asked Dr. Inoue to analyze the ultrastructure of the paranodal junctions in the CD9-deficient mice by electron microscopy. As shown in Figure 3a, paranodal loops were arrayed sequentially and in close apposition to the axonal membrane in the optic nerve of wild-type mice. Between the loops and axolemma, periodic densities corresponding to the transverse bands were apparent (Fig. 3c arrowheads). In contrast, in the optic nerve of mice lacking CD9, the paranodal morphology was frequently perturbed; paranodal loops faced away from the axonal membrane, the transverse bands disappeared entirely and axo-glial junction was completely disrupted (Fig. 3b, arrowheads). Interestingly, some loops occasionally retained a close association with the axon, however, even in these regions, transverse bands disappeared completely (Fig. 3d arrowheads). Figure 3e, f showed that there were no significant changes in the compact myelin between mutant (f) and wild type control (e).

Aberrant localization of axonal domain components in CD9-deficient mice

The findings using mice lacking CD9 strongly suggested that the TM4SF CD9 may have a crucial role for formation of paranodal axoglial junction. To determine whether CD9 has any effect on organization of axonal domains, I analyzed the distribution of paranodal protein Caspr as well as ion channels in mice lacking CD9. In the CNS (optic nerve) and PNS (spinal root) from wild-type mice, Na^+ channels were concentrated in the node of Ranvier and the Kv1.1 potassium channel α subunit was localized at the juxtaparanodal regions, which were adjacent to the paranodal regions as described previously (Fig. 4a, c). In contrast, the localization and shapes of both channel clusters were altered in the CNS and PNS from the CD9-deficient mice

(Fig. 4b, d). In mutant mice, irregular form of Na^+ channel clusters such as binary shape (Fig. 4d) was occasionally observed. Furthermore, the K^+ channel clusters frequently accumulated both in the paranodal region adjacent to the Na^+ channel clusters and the juxtaparanodal regions (Fig. 4d), although such intense labeling in the paranode was never observed in the wild type (Fig. 4a). Heminodal formation that labeled just one side of the juxtaparanode with the antibody against Kv1.1 was also observed in the CD9-deficient mice (Fig. 4b). The staining patterns using the antibodies against other K^+ channel subunits, Kv1.2 and Kvβ2, gave the same results (data not shown).

In addition, to determine the distribution of the axonal paranodal protein Caspr, optic nerve and spinal root were double-labeled for Kv1.1 and Caspr immunoreactivity. In controls, the paired patterns of these proteins were observed next to the unlabeled node in the middle (Fig. 5a, d). In contrast, this type of paired staining was disrupted in the CD9-deficient mice, and Caspr appeared to be diffusely distributed along the axons as shown in Figure 5b and c (optic nerve), and e (spinal root) both in the CNS and PNS.

Altered distribution of axonal domain components in the PNS from CST-deficient mice

As already described in Chapter I, the CST-deficient mice CNS revealed aberrant organization of the axonal domains. To understand the function of myelin sufatide in the characteristic domain formation of the PNS axons, I analyzed the localization of axonal proteins in the spinal roots of the CST-deficient mice. The characteristic channel distribution was observed in the wild type spinal root as shown in Fig. 6a. As

for Na^+ channels, although the elongated Na^+ channel clusters were sometimes observed, these clusters tended to be maintained compared to those of the CNS axons. In contrast, K^+ channels were accumulated markedly in the presumptive paranodal as well as the juxtaparanodal regions in the CST-deficient mice (Fig. 6b) and the stained area occasionally overlapped with those of Na^+ channels in the mutant spinal roots (Fig. 6b). The same staining pattern was obtained using the antibodies against other potassium channel subunits, Kv1.2 and Kv β2 (data not shown). In contrast to the wild type control (Fig. 6c), characteristic distribution of Caspr disappeared in the CST-deficient mice and this protein appeared to be diffusely distributed along the axons as shown in Figure 6d. These changes were quite similar to those in the CNS (Chapter I, Fig. 9, 10). Thus, two myelin molecules, CD9 and sulfatide, are both necessary for the proper domain formation of both PNS and CNS axons.

NF155 is mislocalized in the absence of the axo-glial paranodal junction

The disruption of the paranodal junction caused by the absence of myelin molecules resulted in the abnormal distribution of axonal protein, Caspr. It was of interest to investigate how this junction disruption affected the glial paranodal molecule, NF155 (Tait et al., 2000). Therefore, I examined the distribution of NF155 in the CD9-deficient and CST-deficient mice. NF155 (green) and Caspr (red) were colocalized at the paranodal regions in optic nerve of wild type mouse (Fig. 7a). In contrast, both NF155 and Caspr were hardly detected in the paranodal regions in the CD9-deficient mice (Fig. 7b). These proteins still colocalized at some remaining clusters in presumptive paranodal regions. Furthermore, in the CST-deficient mice, the clusters of NF155 were markedly reduced in number compared to those in the CST-deficient

mice (Fig.7c). These results were similar to the findings in the CGT-deficient mice (Poliak et al., 2001). These results suggested that these two glial paranodal molecules, sulfatide and CD9, are essential not only for the formation of paranodal junctions but also for targeting of NF155 into the paranodal regions.

Discussion

Possible roles of sulfatide and CD9 in the axo-glial junction formation

The present histochemical experiments revealed the importance of two myelin molecules, sulfatide and CD9, in the formation of the paranodal axo-glial junction. CD9 is a TM4SF protein, whereas sulfatide is one of the major myelin glycolipids. How do these two molecules mediate the formation of the paranodal junctions? As described previously, the paranodal junctions bear a strong morphological similarity to the septate junctions found in invertebrates (Rosenbluth et al., 1976). The septate junctions are formed within the ensheathing glia cells that surround the nerve bundles in Drosophila and are essential for establishment of the blood-nerve barrier (Carlson et al., 1997). Recent progress in the genetic and molecular analysis of the septate junction in Drosophila helps us to understand molecular organization of this junction in other species (Brophy, 2001; Hong et al., 2001). The septate junctions are organized by protein complex including transmembrane proteins such as DE-cadherin, Crumbs, and Neurexin IV (Tepass et al., 2001). Actually, Caspr exhibits a significant homology to Drosophila Neurexin IV (Baumagartner et al., 1996), suggesting that the junctions in vertebrates and invertebrates may have common features even at the molecular level.

An interesting possible function of sulfatide is its involvement in protein transport to the myelin membrane and to the paranodal loops. Glycosphingolipid-cholesterol-rich membrane domains in the plasma membrane, termed lipid rafts, can carry membrane proteins to their appropriate destinations within the cell (Simons and Ikonen, 1997). Glycolipids are actively involved in selecting certain proteins for

subcellular transport via detergent-insoluble glycolipid-enriched complexes (DIGs), are thought to be a similar structure as lipid rafts (Ledesma et al., 1998). Myelin sheath is highly enriched in two glycosphingolipids (GalC and sulfatide) as well as cholesterol, suggesting that rafts containing these lipids may play significant roles in myelin assembly as reported recently by Simons et al (2000). Thus, sulfatide may induce formation of DIGs in which some adhesion molecules would be enriched and be transported selectively to the paranodes to form the axo-glial junctions.

A characteristic feature of TM4SF including CD9 is to form complexes with a variety of membrane proteins. They have short cytoplasmic amino and carboxyl termini and a short cytoplasmic loop, all of which lack any obvious signaling motifs (Berditchevski et al., 1996). These TM4SF proteins are thus supposed to work as "adapters for membrane proteins" or "molecular facilitators" which mediate the formation of large molecular complexes to allow them to function more efficiently (Nakamura et al., 2000). Interestingly, CD9 is known to bind with the membrane-anchored form of heparin-binding EGF-like growth factor (proHB-EGF) and up-regulates its binding activity to the ligand (Iwamoto et al., 1994; Higashiyama et al., 1995). Thus, CD9 at the paranodal regions may possibly form a complex with other components in this region, and may modulate their functions. Furthermore, recent literatures demonstrated that CD9 was localized in the lipid raft domains on the T cell surface (Yashiro-Ohtani et al., 2000). Taken together, CD9 may interact with other glial paranodal proteins, which are targeted to the paranodal loops by incorporation into the lipid rafts. Glial cell adhesion molecule NF155 may be one of these proteins, since its transport to the paranode was severely disturbed by lack of either molecule from myelin (Fig. 7). Even though it is still possible that the disruption of paranodal

junction itself might cause the mislocalization of NF155, the present observations more strongly suggest that the complex containing CD9 and adhesion molecule NF155 are incorporated into the lipid rafts formed in the presence of sulfatide and are transported to the paranodal loops to form axo-glial junctions. At the paranode, CD9 may upregulate the binding activity of NF155 to some axonal molecules.

Molecular mechanisms underlying formation of the axo-glial paranodal junctions

Major defects of the CD9-deficient and CST-deficient mice were the complete absence of transverse bands and the abnormal lateral loops frequently turned away from the axon (Chapter I Fig. 8b, Chapter II Fig. 2b, d). Furthermore, these mutants showed aberrant localization of K^+ channel clusters at the presumptive paranodal regions and immature Na^+ channel clusters both in the CNS and PNS (Fig.9, 10 in Chapter I; Fig.4, 5, 6 in Chapter II). Currently, in addition to these two mutants, three different mouse mutants are available for studying the molecular composition and functional roles of the paranodal regions. One of the mutants is characterized by deficiency of the major myelin glycolipids, GalC and sulfatide (see Introduction; Coetzee et al., 1996), and other two mutants lack one of the axonal paranodal proteins, Caspr (Bhat et al., 2001) or contactin (Boyle et al., 2001; Poliak et al., 2001). All these mutants primarily exhibit disruption of the paranodal axo-glial junctions as shown by electron microscopic studies, and changes of axonal protein localization around the nodes. However, the structure of the compact myelin is intact in all of these mutants.

Contactin is a GPI-linked membrane protein involved in the junctional formation. As it is anchored only to the extracellular side of the plasma membrane, contactin should interact with laterally associated membrane proteins to convey signals

into the cell. As expected, contactin and Caspr form a *cis* complex within the paranodal axolemma (Peles et al., 1997). Formation of such a contactin-Caspr complex is independent of myelin-inducing signals. The complex is formed before reaching the cell surface and is transported to the cell surface by contactin- mediated signals (Rios et al., 2000). Thus, Caspr is completely eliminated from the axolemma in contactin-deficient mutants. In the absence of Caspr, contactin is transported to the axolemma but is undetectable at the paranodes (Bhat et al., 2001). These studies therefore cannot discern the separate contributions of contactin and Caspr in the paranodal organization.

On the other hand, from immunohistochemical analysis (Fig. 4, 5), the aberrant distribution of axonal proteins in the CD9-deficient mice was milder than that in CST-deficient mice. It is well known that a member of TM4SF often forms complexes with other TM4SF proteins on the cell surface (Stipp et al., 2001; Hemler 2001). As discussed before, TM4SF proteins may act as facilitator or adaptors for connecting a subset of cell-surface proteins to a network, termed as a tetraspan web. Thus it is possible that CD9 at the paranodal region may associate with other member of TM4SF, and therefore the loss of CD9 caused less damage compare to those of other paranodal molecules. Another myelin cell adhesion molecule in the paranodal junctions is NF155. The carboxy terminus of this protein contains an ankyrin-binding site where its binding ability is regulated by tyrosin phosphorylation (Davis et al., 1994, 1996; Michaely et al., 1995). Therefore, NF155 is a strong candidate to mediate the axo-glial interaction, although the axonal ligand of this molecule has not been identified yet. Actually in the CD9-deficient and CST-deficient mice, NF155 was hardly detected in the paranodal regions (Fig. 7). In contactin-deficient mutant, in contrast, NF155 was

retained within the paranodal region, although the staining intensity was weaker than that in wild type mice (Boyle et al., 2001).

Both axonal mutants, Caspr-deficient and contactin-deficient mice, displayed severe neurological deficits. Myelin lipid mutants, CST-deficient mice, also exhibited clearly neurological deficits. However CD9-deficient mice displayed no apparent neurological deficit, which support the idea described above that other TM4SF proteins, yet to be identified, may associate with them which can compensate its absence. Taken together, CD9 and other unknown TM4SF proteins may interact with glial adhesion molecules including NF155 and the targeting of such complex to the paranodal myelin loops may require sulfatides. As soon as such a myelin complex is targeted to the paranode, the contactin-Caspr complex may be concentrated at the axonal side of the paranode to complete the axo-glial junction formation. Based on our present experiments, future studies identifying of other components in the paranodal CD9 complex including glial ligands for the contactin-Caspr complex should clarify how these junctions are assembled.

Materials and Methods

Animals

ICR mice were purchased from Japan SLC Inc. (Hamamatsu, Japan). The *jimpy* (jp/Y) mutant mice (B6CBA/J-jp) were originally obtained from Jackson Laboratories (Nave et al., 1987). The transgenic mouse line (4e) was generated by introducing a cosmid clone containing the entire mouse proteolipid protein (PLP) gene (Kagawa et al., 1994). Both mouse lines were maintained in the animal facility in the National Institute for Physiological Sciences. Galactosylceramide sulfotransferase (CST)-deficient mice were produced by gene targeting (Honke et al., submitted). The targeting construct was designed to replace the exon portions encoding the transmembrane domain and the 3' -phosphoadenosine 5' -phosphosulfate (PAPS)-binding motif in the CST gene with a neomycin-resistance cassette. The mouse line was maintained in the animal facility in Osaka Medical Center for Maternal and Child Health. CD9 knockout mice were also created by gene targeting (Miyado et al., 2000) and the mouse line was maintained in the National Institute for Physiological Sciences. These genetic types of *jimpy*, PLP transgenic mice (*tg*), CST-deficeint and CD9-deficient mice were determined by the polymerase chain reaction (PCR) method using specific primers.

Antibodies

Rabbit polyclonal antibody against Na^+ channels was generated using synthetic peptides of a highly conserved 18-amino acid segment (TEEQKKYYNAMKKLGSKK) between homologous domains III and IV in the Na^+

channel α-subunit (synthesized at Peptide Institute, Inc, Japan) as an antigen. A cysteine residue was added to the C terminus of this peptide to form conjugates with keyhole limpet hemocyanin (KLH) using Imject Maleimide activated mc KLH kit (Pierce). The polyclonal antibody was raised in rabbits (Sawady Technology), followed by affinity purification by immunoabsorption to a peptide-coupled column (Sulfolink Kit, Pierce). For NF155 localization, rabbit polyclonal antibody was generated against a synthetic peptides (LWVSQKRQQASFPGDRPR) (Peptide Institute) corresponding to a region at the second to the third FNIII domain specific to NF155 (Tait et al., 2000). A cysteine residue was added to the C terminus of this peptide and linked to KLH as described above. Polyclonal antibody was raised in rabbits (Sawady Technology), followed by affinity purification using a peptide-coupled column as described above. The specificity of this antibody was investigated by Western blotting, absorption test and immunohistochemistry. The anti-Na^+ channel and anti-NF155 antibodies were used at a dilution of 1:100 and 1:150, respectively. The polyclonal and monoclonal antibodies against K^+ channel α- and β-subunits (Trimmer, 1991) were kindly provided by Dr. J.S. Trimmer (State University of New York at Stony Brook, NY) and were used at a dilution of 1:100. The polyclonal and monoclonal anti-Caspr antibodies were kindly gifted by Dr. Peles (The Weizmann Inst., Israel) and used at a dilution of 1:2,500 and 1:250, respectively (Peles et al., 1997). A mouse monoclonal antibody against $ankyrin_G$ was purchased from Zymed Laboratories (San Francisco, USA) and used at a dilution of 1:250. A mouse monoclonal antibody against myelin basic protein (MBP) was purchased from Boehringer-Mannheim (Mannheim, Germany) and used at a dilution of 1:200. A rat monoclonal antibody (AA3) against the C-terminal portion of myelin proteolipid protein (PLP) (Yamamura

et al., 1991) was kindly provided by Dr. M. Lees (EK Shriver Center, Waltham, MA) and used at a dilution of 1:100.

Immunohistochemistry

Animals were fixed by transcardial perfusion with 4% paraformaldehyde in 0.1 M phosphate buffer (PB), pH7.4 (1ml/g body weight). Immediately after perfusion, the eyes together with the proximal portion of the optic nerve and separate distal portions of the optic nerve and cervical (C3-C5) spinal cords were dissected out. The tissues were cryoprotected by immersion for 2-3 hours in 10% sucrose in 0.01 M phosphate buffered saline (PBS), pH7.4, followed by 30% sucrose in PBS, pH7.4, overnight at 4°C. After embedding in OCT mounting medium (Miles, Elkhart, IN), the blocks were cut in 7-μm-thick sections. The sections were collected on 3-aminopropyltriethoxysilane (silan) (Sigma Chemical Co.) rubbed glass slides and allowed to air dry. Before incubation with the NF155 antibody, sections were treated with Bouin's regent (0.9% Picric acid, 9% formaldehyde, and 5% acetic acid) for 1 min. After washing in PBS to remove OCT, the sections were permeabilized for 2hr in 0.1 M PB, containing 0.3% Triton X-100 and 10% goat serum, pH7.4, (PBTGS). For single or double-labeling experiments, sections were incubated overnight at 4°C with primary antibodies diluted to appropriate concentrations in PBTGS. Then the sections were thoroughly rinsed in PBS, followed by the application of fluorescently labeled secondary antibodies for 40 min at room temperature (RT). Alexa 488-conjugated (1:1,500; Molecular Probes) or FITC-conjugated (1:400; Cappel Laboratories) secondary antibodies were used to detect rabbit polyclonal antibodies; Alexa 568-conjugated (1:1,500; Molecular Probes) or TRITC-conjugated (1:400;

Jackson ImmunoResearch) secondary antibodies were used to detect monoclonal antibodies. Finally, labeled sections were rinsed consecutively in PBTGS, 0.1 M PB, and 0.05 M PB for 5 min each, and were mounted in Vectashield medium (Vector Laboratories, CA). Images were captured with a laser scanning microscope LSM510 (Carl Zeiss) and the confocal images were acquired. They were initially processed using LSM software and later exported into Adobe Photoshop 6.0 for final processing.

Quantification of ion channel clusters and cluster lengths of Na^+ channel

A focal region of immunofluorescence was considered to represent a cluster (aggregate) of Na^+ or K^+ channels if (1) it clearly stood out from background label, and (2) the fluorescence intensity was 150 or more using LSM510 software (Carl Zeiss). Based on the criteria mentioned above, the cluster numbers of ion channels were counted and the length of each Na^+ channel cluster was measured by digital linear gauges using LSM510 software. Gauge outputs were transferred to a laboratory computer, and at least two sections of nerve from each animal were analyzed.

Preparation of brain and optic nerve homogenate

The mice (PLP *tg* heterozygous and littermate control mice) were deeply anesthetized by intraperitoneal administration of sodium pentobarbital. Brains and optic nerves were removed, homogenized in lysis buffer (25 mM HEPES, 300mM NaCl, 1.5 mM $MgCl_2$, 0.2 mM EDTA, pH 8.0, 0.1% Triton X-100, 20 mM β-glycerophosphate, 2 μg/ml leupeptin, 0.5mM DTT, pH 7.7), and the protein concentrations were measured by Bio-Rad Potein Assay (Bio-Rad Laboratories).

Purification of myelin

Myelin purification was carried out using the method modified from Norton & Poduslo (1973) and Huber et al. (1994). All the purification steps and protein handling were performed at 4°C or on ice. Briefly, cerebral cortex, medulla oblongata and spinal cord from 18-week-old mice (CST-deficient and littermate control mice) were homogenized in 19 volumes of 0.85 M sucrose/ 2 mM O,O-bis (2-aminoethyl) ethyleneglycol-N,N,N'-N'-tetraacetic acid (EGTA), pH 7.5, with a Glass-Tefron Potter homogenizer with 10 strokes at 850 rpm. The homogenate was overlaid with 16.5 ml of 0.32 M sucrose/ 2mM EGTA and ultracentrifuged at 28,000 rpm for 60 min in an SW-28 rotor (Beckman). The interface of 0.85/ 0.32 M sucrose was collected, resuspended in 20 ml distilled H_2O and centrifuged at 30,000 rpm in a Type 50.2 Ti rotor (Beckman). The pellet was resuspended in 20 ml of 10 mM EGTA, pH 7.5, and homogenized. The susupension was kept at 2°C and centrifuged at 10,000 rpm for 15 min in a JA-17 fixed angle rotor (Beckman). The pellet was washed again under the same conditions. The pellet was homogenized in 17 ml of 0.85 M sucrose/ 2 mM EGTA, pH 7.5, overlaid with 18 ml of 0.32 M sucrose/ 2 mM EGTA, pH 7.5, and centrifuged at 28,000 rpm for overnight in an SW-28 rotor. The interface was collected by centrifugation and washed repeatedly. The suspention was kept at 2°C and centrifuged at 10,000 rpm for 15 min in a JA-17 fixed angle rotor. The pellet (myelin fraction) was homogenized in 3 ml of 1 mM EDTA, 1 mM EGTA, 10 μM pepstatin A, 10 μM leupeptin, 0.1 mM PMSF, 50 mM Tris-HCl, pH 7.5, aliquoted, snap frozen in liquid N_2 and stored at –80°C. Protein concentration of the myelin fraction was determined using the Bradford method (Bio-Rad).

SDS-PAGE and Western blotting analysis

Each sample (5-20 μg) was analyzed by 7.5% or 15% SDS-polyacrylamide gel electrophoresis (SDS-PAGE) and electroblotted to nitrocellulose (Millipore) or PVDF membranes (Amersham Pharmacia) in a tank transfer system (Bio-Rad). Blots were blocked with 5% nonfat milk in 10mM Tris-HCl, 100mM NaCl, and 0.1% Tween 20, pH 7.5, (blocking buffer) for 1hr at RT and probed with anti-Kv1.1 and-Kvβ2 antibodies (1:200), anti-Caspr (1:3,000), anti-MBP (1:3,000), and anti-PLP (1:1,000) antibodies. They were washed with 10 mM Tris-HCl containing 0.1% Tween 20, pH 7.5, (TBS-T) and exposed to either goat anti-rabbit, mouse or rat IgG conjugated by horseradish peroxidase (HRP) (Santa Cruz Bio.) diluted in blocking buffer for 30 min at RT, respectively. After being washed thoroughly, immunoreactive bands were visualized using the ECL system (Amersham Pharmacia) according to the manufacturer's instructions.

Preparation of teased sciatic nerves

Developing (P0, P1, P2, P4, P6, P8, and P10) and adult sciatic nerves were dissected immediately without perfusion, desheathed, and incubated with collagenase (2.0-3.6mg/ml; Sigma Chemical Co.) for 1 hr at RT. Using fine needle, the individual nerves were dissociated and teased gently in ice-cold PBS, pH 7.4. Then, the separated fibers were spread on silan-coated glass slides and fixed by 4% paraformaldehyde in 0.1 M PB, pH 7.4, for 15-30 min, rinsed in 0.05 M PB, pH 7.4, for 10 min, and air-dried. The slides were stored at –80°C until they were stained for immunofluorescence.

Acknowledgements

I would like to express my sincere appreciation to Professor Kazuhiro Ikenaka and Professor Hiroko Baba (Tokyo University of Pharmacy and Life Science) for their generous support and valuable guidance throughout this study. I am also sincerely grateful to Dr. Hitoo Nishino (Nagoya City University), Dr. Keiji Imoto, and Dr. Kensuke Nakahira (Saitama Medical School) for their helpful discussion and advice.

I am thankful to Dr. Yoshiro Inoue and Dr. Masahiko Watanabe (Hokkaido University) for kindly providing me electron microscopic analysis of CD9-deficient mouse. I also would like to thank Dr. Jeffrey L. Dupree (Eastern Virginia Medical School) for kindly providing me electron microscopic analysis of CST-deficient mouse. I deeply appreciate the Electron Microscopy Room at the National Institute for Physiological Sciences for using microscopic to observation in this work. I would like to thank Dr. Elior Peles (The Weizmann Institute of Science, Israel) for providing with anti-Caspr antibody, and also thank Dr. James S. Trimmer (SUNY at Stony Brook) for kindly providing me with anti-Kv1.1 antibody, anti-Kv1.2 antibody and ant-Kvβ2 antibody. Further, I would like to thank Dr. Koichi Honke (Osaka University) and Dr. Eisuke Mekada (Osaka University) for kindly providing me with CST-deficient and CD9-deficient mice, respectively. I appreciate deeply that Dr. Yukie Hirahara (Tront University) maintained the CST-deficient mouse and I also appreciate that Ms. Rie Taguchi maintained all other mice.

I with to thank all the members of Laboratory of Neural Information at the National Institute for Physiological Sciences, Department of Physiology at Nagoya City University Medical School, and Department of Molecular Neurobiology at Tokyo University of Pharmacy and Life Science. Finally, I also appreciate my parents from the bottom of my heart for supporting me everything without any compensation.

References

Anton ES, Hadjiargyrou M, Patterson PH, a Matthew WD (1995) CD9 plays role in Schwann cell migration in vitro. J Neurosci 15:584-595.

Arroyo E.J, Xu T, Grinspan, J, Lambert S, Levinson SR, Brophy PJ, Peles E, Scherer SS (2002) Genetic dysmyelination alters the molecular architecture of the nodal region. J Neurosci. 22:1726-1737.

Baba H, Akita H, Ishibashi T, Inoue Y, Nakahira K, Ikenaka K (1999) Completion of myelin compaction, but not the attachment of oligodendroglial processes triggers K+ channel clustering. J Neurosci Res 58:752-764.

Baumagartner S, Littleton JT, Broadie K Bhat MA, Herbecke R, Lengyel JA Chiquet-Ehrismann R, Prokop A, Bellen HJ (1996) A drosophila neurexin is required for septate junction and blood-nerve barrier formation and function. Cell 87:1059-1068.

Bennett V, Lambert S (1999) Physiological roles of axonal ankyrins in survival of premyelinated axons and localization of voltage-gated sodium channels. J Neurocytol 28:303-318.

Berditchevski F, Zutter MM, Hemler ME (1996) Characterization of novel complexes on the cell surface between integins and proteins with 4 transmembrane domains (TM4 proteins). Mol Biol Cell 7:193-207.

Berglund EO, Ranscht B (1994) Molecular cloning and in situ localization of the human contactin gene (CNTN1) on chromosome 12q11-q12. Genomics 21:571-582.

Bhat MA, Rios JC, Lu Y, Garcia-Fresco GP, Ching W, Martine MS, Li J, Einheber S, Chesler M, Rosenbluth J, Salzer JL, Bellen HJ (2001) Axo-glial interactions and the domain organization of myelinated axons requires neurexin 4/Caspr/Paranodin. Neuron 30:369-383.

Bosio A, Binczek E, Stoffle W (1996) Fuctional breakdown of the lipid bilayer of the myelin

membrane in central and peripheral nervous system by disrupted galactocerebroside synthesis. Pros Natl Acad Sci USA 12:13280-13285.

Boucheix C, Benoit P (1988) CD9 antigen: will platelet physiology help o explain the function of surface molecule during hemopoietic differentiation? Nouv Rev Fr Hematol 30:201-202.

Boyle MET, Berglund EO, Murai KK, Weber L, Peles E, Ranscht B (2001) Contactin orchestrates assembly of septate-like junctions at the paranode in myelinated peripheral nerve. Neuron 30:385-397.

Brophy PJ (2001) Axoglial junctions: Separate the channels or scramble the message. Current Bio 11:555-557.

Carlson SD, Hilgers SL, Juang JL (1997) Ultrastructure and blood-nerve barrier of chordotonal organs in the Drosophila embryo. J Neurocytol 26:377-388.

Coetzee T, Fujita N, Dupree J, Shi R, Bright A, Suzuki K, Popko B (1996) Myelination in the absence of galactocerebroside and sulfatide: normal structure and abnormal function and regional instability. Cell 86:209-219.

Davis JQ and Bennett V (1994) Ankyrin-binding activity shared by the neurofascin/L/NrCAM family of nervous system cell adhesion molecules. J Biol Chem 269:27163-27166.

Davis JQ, Lambert S, Bennett V (1996) Molecular composition of the node of Ranvier : identification of ankyrin-binding cell adhesion molecules neurofascin (mucin+/third FN III domain-) and NrCAM at nodal axon segments. J Cell Biol 135:1355-1367.

Deerinck TJ, Levinson RS, Bennett VG, Ellisman MH (1997) Clustering of voltage-sensitive sodium channels on axons is independent of direct Schwann cell contact in the dystrophic mouse. J Neurosci 17:5080-5088.

Dentinger MP, Barron KD, Csiza CS (1982) Ultrastructure of the CNS in a myelin-deficient rat. J Neurocytol 11:671-691.

Dugandzija-Novakovic S, Koszowski AG, Levinson RS, Shrager P (1995) Clustering of Na^+ channels and node of Ranvier formation in remyelianting axons. J Neurosci 15:492-503.

Duncan ID, Hammang JP, Goda S, Quarles RH (1989) Myelination in the jimpy mouse in the absence of proteolipid protein. Glia 2:148-154.

Dupree JL, Girault J-A, Popko B (1999) Axo-glial interactions regulate the localization of axonal paranodal proteins. J Cell Biol 147: 1145-1151.

Einheber S, Zanazzi G, Ching W, Scherer S, Milner T.A, Peles E, Salzer J.L (1997) The axonal membrane protein Caspr, a homologue of neurexin IV, is a component of the septate-like paranodal junctions that assemble during myrlination. J Cell Biol. 139:1495-1506.

Faivre-Sarrailh C, Gauthier F, Denisenko-Nehrbass N, Bivic A, Rougon G, Girault JA (2000) The glycosylphosphatidyl inositol-anchored adhesion molecule F3/contaction is required for surface transport of paranodin/contactin –associated protein (caspr). J Cell Biol 149:491-501.

Hemler ME. (2001) Specific tetraspanin functions. J Cell Biol. 155:1103-1107.

Higashiyama S, Iwamoto R, Goishi K, Raab G, Taniguchi N, Klagsbrun M, Mekada E (1995) The membrane protein CD9/DRAP27 potentiates the juxtacrine growth factor activity of the membrane-anchored heparin-binding EGF-like growth factor. J Cell Biol 128:929-938.

Hirano A, Dembitzer HM (1982) Further studies on the transverse bands. J Neurocytol 11:851-856.

Hong Y, Stronach B, Perrimon N, Lily YJ, Yuh NJ (2001) *Drosophila* stardust interacts with crumbs to control polarity of epithelia but not neuroblasts. Nature 414:634-638.

Honke K, Hirahara Y, Dupree J, Suzuki K, Popko B, Fukushima J, Nagasawa T, Yoshida N, Wada Y, Taniguchi N (2002) Paranodal junction formation and spamatogenesis require sulfoglycolipids. Proc Natl Acad Sci (in press).

Huber LA, Madison DL, Simons K, Pfeiffer SE (1994) Myelin membrane biologenesis by oligodendroceytes: developmental regulation of low-molecular weight GTP-binding proteins. FEBS Lett 347:273-278.

Inoue Y, Nakamura R, Mikoshiba K, Tsukada Y (1981) Fine structure of the central myelin sheath in the myelin deficient mutant Shiverer mouse, with special reference to the pattern of myelin formation by oligodendroglia. Brain Res 219:85-94.

Inoue Y, Kagawa T, Matsumura Y, Ikenaka K, Mikohsiba K (1996) Cell death of oligodendrocytes or demyelination indeuced by overexpression of proteolipid protein depending on expressed gene dosage. Neurosci Res 25:161-172.

Iwamoto R, Higashiyama S, Mitamura T, Taniguchi N, Klagsbrun M, Mekada E (1994) Heparin-binding EGF-like growth factor, which acts as the diphtheria toxin receptor, forms a complex with membrane protein DRAP27/CD9, which up-regulates functional receptors and diphtheria toxin sensitivity. EMBO J 13:2322-2330.

Jenkins SM, Bennett V. (2002) Developing nodes of Ranvier are defined by ankyrin-G clustering and are independent of paranodal axoglial adhesion. Proc. Natl. Acad. Sci. 99:2303-2308.

Kagawa T, Ikenaka K, Inoue Y, Kuriyama S, Tsuji T, Nakao J, Nakajima K, Aruga J, Okano H, Mikoshiba K (1994) Glial cell degeneration and hypomyelination caused by overexpression of myelin proteolipid protein gene. Neuron 13:427-442.

Kagawa T, Mekada E, Shishido Y, Ikenaka K (1997) Immune system-related CD9 is expressed in mouse central nervous system myelin at a very late stage of myelination. J Neurosci Res 50:312-320.

Kaplan MR, Meyer-Franke A, Lambert S, Bennet V, Duncan ID, Levinson SR, Barres BA (1997) Induction of sodium channel clustering by oligodendrocytes. Nature 136:724-728.

Kim E, Niethammer M, Rothschild A, Jan YN, Sheng M (1995) Clustering of Shaker-type K^+ channels by interaction with a family of membrane-associated guanylate kinases. Nature 378:85-88.

Knapp PE, Skoff RP (1987) A defect in the cell cycle of neuroglia in the myelin deficient jimpy mouse. Dev. Brain Res 35:301-306.

Kordeli E, Lambert S, Bennett V (1995) AnkyrinG. A new ankyrin gene with neural –specific isoforms localized at the axonal initial segment and node of Ranvier. J Biol Chem 270:2354-2359.

Lambert S, Davis JQ, Bennett V (1997) Morphogenesis of the node of Ranvier; co-clusters of ankyrin and ankyrin-binding integral proteins define early developmental intermediates. J Nuerosci 17:7025-7036.

Ledesma MD, Simons K, Dotti CG (1998) Neuronal polarity: essential role of protein-lipid complexes in axonal sorting. Proc Natl Acad Sci 95: 3966-3971.

Maecker HT, Todd SC, Levy S (1997) The tetraspanin superfamily: molecular facilitator. FASEB J 11:428-442.

Martin S, Levine AK, Chen ZJ, Ughrin Y, Vevine JM (2001) Deposition of the NG2 proteoglycan at nodes of Ranvier in the peripheral nervous system. J neurosci 21:8119-8128.

Mathis C, Denisenko-Nehrbass N, Girault JA, Borrelli E. (2001) Essential role of oligodendrocytes in the formation and maintenance of central nervous system nodal regions. Development 128:4881-4890.

Michaely P, Bennett V (1995) Mechanism for binding site diversity on ankyrin. Comparison of binding sites on ankyrin for neurofascin and the Cl-/HCO3- anion exchanger. J Biol Chem 270:31298-31302.

Miyado K, Yamada G, Yamada S, Hasuwa H, Nakamura Y, Ryu F, Suzuki K, Kosai K, Inoue K, Ogura A, Okaba M, Mekada E (2000) Requirement of CD9 on the egg plasma membrane for fertilization. Science 287:321-324.

Morell P, Radin NS (1969) Synthesis of cerebroside by brain from urdine diphosphate galactose and ceramide containing hydroxy fatty acid. Biochem 8:506-512.

Nakamura Y, Iwamoto R, Mekada E (1995) Membrane-anchored heparin-binding EGF-like growth factor (HB-EGF) and diphtheria toxin receptor-associated protein (DRAP27)/CD9

from a complex with integrin alpha 3 beta 1 at cell-cell contact sites. J Cell Biol 129:1691-1705.

Nakamura Y, Iwamoto R, Mekada E (1996) Expression and distribution of CD9 in myelin of the central and peripheral nervous systems. Am J Pathol 149:575-583.

Nakamura K, Mitamura T, Takahashi T, Kobayashi T, Mekada E (2000) Importance of the major extracellular domain of CD9 and the epidermal growth factor (EGF)-like domain of heparin-binding EGF-like growth factor for up-regulation of binding and activity. J Biol Chem 275:18284-18290.

Nave KA, Bloom FE, Milner RJ (1987) A single nucleotide difference in the gene for myelin proteolipid protein defines the jimpy mutation in mouse. J Nuerochem 49:1873-1877.

Norton WT, Poduslo SE (1973) Myelination in rat brain: method of myelin isolation. J Neurochem 21:749-757.

Pedraza L, Huang JK, Colman DR (2001) Organizing principles of the axoglial apparatus. Neuron 30:335-344.

Peles, E., Nativ, M., Lustig, M., Grumet, M., Schilling, J., Martinez, R., Plowman, G. D., and Schlessinger, J. (1997). Identification of a novel contactin-associated transmembrane receptor with multiple domains implicated in protein-protein interactions. EMBO J 16:978-988.

Poliak S, Gollan L, Martinez R, Custer A, Einheber S, Salzer JL, Trimmer JS, Shrager P, Peles E (1999) Caspr2, a new member of the neurexin superfamily, is localized at the juxtaparanodes of myelinated axons and associates with K+ channels. Neuron 24:1037-1047.

Poliak S, Gollan L, Salomon D, Berglund EO, Ohara R, Ranscht B, Peles E (2001) Localization of Caspr2 in myelinated nerves depends on axo-glia interactions and the generation of barriers along the axon. J Neurosci 21:7568-7575.

Rasband MN, Trimmer JS, Schwarz TL, Levinson SR, Ellisman MH, Schachner M, Shrager P

(1998) Potasiium channel distribution, clustering, and function in remyelinating rat axons. J Neurosci 18:36-47.

Rasband MN, Peles E, Trimmer JS, Levinson R, Lux SE, Shrager P (1999a) Dependence of nodal sodium channel clustering of paranodal axoglial contact in the developing CNS. J Neurosci 19:7516-7528.

Rasband MN, Trimmer JS, Peles E, Levinson R, Shrager P (1999b) K^+ channel distribution and clustering in developing and hypomyelinatind axons of the optic nerve. J Neurocytol 28:319-331.

Rios JC, Melendez-Vasquez CV, Einheber S, Lustig M, Grumet M, Hemperly J, Peles E, Salzer JL (2000) Contactin-associated protein (Caspr) and contactin from a complex that is targeted to the paranodal junctions during myelination. J Neurosci 20:8354-8364.

Richie JM, Rang HP, Pellegrino R (1981) Sodium and potassium channels in demyelinated and remyelinated mammalian nerve. Nature 294:257-259.

Rosenbluth J (1976) Intramembranous particle distribution at the node of Ranvier and adjacent axolemma in myelinated axons of the frog brain. J Neurocytol 5:731-745.

Rosenbluth J (1980) Central myelin in the mouse mutant shivere. Brain Res 208:283-297.

Rosenbluth J (1995a) Pathology of demyelinated and dysmyelinated axons. In: Kettenmann H, Ransom B, editors. Neuroglia. New york: Oxford UP. P 391-411.

Rosenbluth J (1995b) Glial membranes and axonglial junction. In: Kettenmann H, Ransom B, editors. Neuroglia. New York: Oxford UP. P 613-633.

Salzer JL (1995) Mechanisms of adhesion between axons and glial cells. In The Axon: edited by Waxman S, Kocsis J, Stys P, editors. New York: Oxford Univ. press. P164-179.

Salzer JL (1997) Clustering sodium channels at the node of Ranvier: close encounters of the axo-glia kind. Neuron 18:843-846.

Schmidt C, Kunemund V, Wintergerst ES, Schmitz B, Schachner M (1996) CD9 of mouse brain is implicated in neurite outgrowth and cell migration in vitro and is associated with the

a6/b1 integrin and the neural adhesion molecule L1. J Neurosci Res 43:12-31.

Sheng M, Kim E (1996) Ion channel associated proteins. Curr Opin Neurobiol 6:602-608.

Shrager P (1989) Sodium channels in signal demyelianated mammalian axons. Brain Res 483:149-154.

Simons K, Ikonen E (1997) Functional rafts in cell membranes. Nature 387:569-572.

Simons M, Kramer EM, Thiele C, Stoffel W, Trotter J (2000) Assemble of myelin by association of proteolipid protein with cholesterol-and galactosylceramide-rich membrane domains. J Cell Biol 151:143-154.

Sims TJ, Waxman SG, Black JA, Gilmore SA (1985) Perinodal astrocytic processes at nodes of Ranvier in develop normal and glial cell deficient rat spinal cord. Brain Res 337:321-331.

Srinivasan Y, Elmer L, Davis J, Bennett V, Angelides K (1988) Ankyrin and spectrin associate with voltage-dependent sodium channels in brain. Nature 333:177-180.

Stipp AS, Orlicky D, Hemlar ME (2001) FPRP, a major, highly stoichiometric, highly specific CD81- and CD9-associated protein. J Biol Chem 276:4853-4862.

Tait S, Gunn-Moore F, Collinson JM, Huang J, Lubetzki C, Pedraza L, Sherman DL, Colman DR, Brophy PJ (2000) An oligodendrocyte cell adhesion molecule at the site of assembly of the paranodal axo-glial junction. J Cell Biol 150: 657-666.

Tepass U, Tanentzapf G, Ward R, Fehon R (2001) Epithelia cell polarity and cell junctions in Drosophila. Annu Rev Genet 35:747-784.

Trimmer JS (1991) Immunological identification and characterization of a delayed rectifier K^+ channels polypeptide in rat brain. Proc Natl Acad Sci USA 88:10764-10768.

Vabnick I, Novakivuc SD, Levinson SR, Schachner M, Schrager P (1996) The clustering of axonal sodium channels during development of the peripheral nervous system. J Neurosci 16:4914-4922.

Vabnick I, Trimmer JS, Schwarz TL, Levinson SR, Risal D, Shrager P (1999) Dynamic potassium channel distributions during axonal development prevent aberrant firing patterns.

J Neurosci 19:747-758.

Wang H, Kunkel DD, Martin TM, Schwartzkroin PA, Tempel BL (1993) Heteromultimeric K^+ channels in terminal and juxtaparanodal regions of neurons. Nature 365:75-79.

Wang H, Allem ML, Grigg JJ, Noebels JL, Tempel BL (1995) Hypomyelination alters K^+ channel expression in mouse mutants *shiverer* and *Trembler*. Neuron 15:1337-1347.

Waxman SG and Black JA (1995) Axoglial interactions at the cellular and molecular levels in central nervous system myelinated fibers. In Neuroglia: edited by Kettenmann H and Ransom BR. New York: Oxford Univ. Press. P587-610.

Wiggins RC, Chongjie G, Delaney C, Samorajski T (1988) Development of axonal-oligodendroglial relationships and junctions during myelination of the optic nerve. Int J Dev Neurosci 6:233-243.

Yamamura T, Konola JT, Wekerle H, Lees MB (1991) Monoclonal antibodies against myelin proteolipid protein: identification and characterization of two major determinants. J Neurochem 57 (5):1671-1680.

Yashiro-Ohtani Y, Zhou X, Toyo-oka K, Tai X, Park C, Hamaoka T, Abe R, Miyake K, Fujiwara F (2000) Non-CD28 costimulatory molecules present in T cell rafts induce T cell costimulation by enhancing the association of TCR with rafts. J Immun 164:1251-1259.

Zhang X, Davis JQ, Carpenter S, Bennett V (1998) Structural requirements for association of neurofascin with ankyrin. J Biol Chem 273:30785-30794.

Zhou D, Lembert S, malen PL, Carpenter S, Boland LM, Bennett V (1998) AnkyrinG is required for clustering of voltage-gated Na channels at axon initial segments and for normal action potential firing. J Cell Bilo 143:1295-1304.

Chapter I

Figures and Figure legends

Figure 1

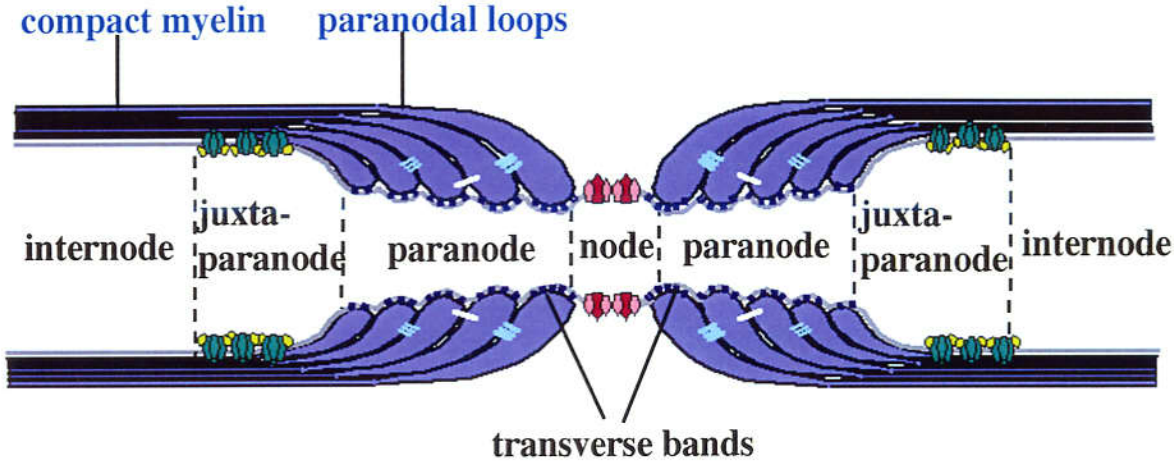

	juxtaparanode	node	paranode
axonal proteins	Caspr2 Kv1.1, 1.2, β2	Na⁺Ch AnkyrinG NrCAM NF186	Caspr contactin
glial protein			neurofascin 155 (NF155)

Figure legends

Chapter I

Figure 1

Longitudinal domains of myelinated axons in the central nervous system (CNS)

A longitudinal section through a myelinated axon at the node is illustrated schematically, indicating the organization and protein composition of axonal domains. Myelin is formed by oligodendrocytes in the CNS. Three distinctive segments are represented; internode, paranode, and node of Ranvier. Only a part of the internode, which is located beneath the compact myelin, is shown. Voltage-gated K^+ channels (Kv1.1, 1.2, β2) and Caspr2 are concentrated in the juxtaparanodal region where is a flanking region of the paranode. At the paranodes, paranodal myelin loops contact with the axolemma to form transverse bands. Caspr and contactin are concentrated at the axonal side proteins and neurofascin 155 (NF155) is at a glial side in this region. At the node, perinodal astroglial processes frequently cover the axolemma (not shown). Intermembranous particles are enriched at the node those are corresponding to voltage-gated Na^+ channels (Na^+ Ch). AnkyrinG and the cell adhesion molecules NrCAM and NF186 are also concentrated in this region.

Figure 2

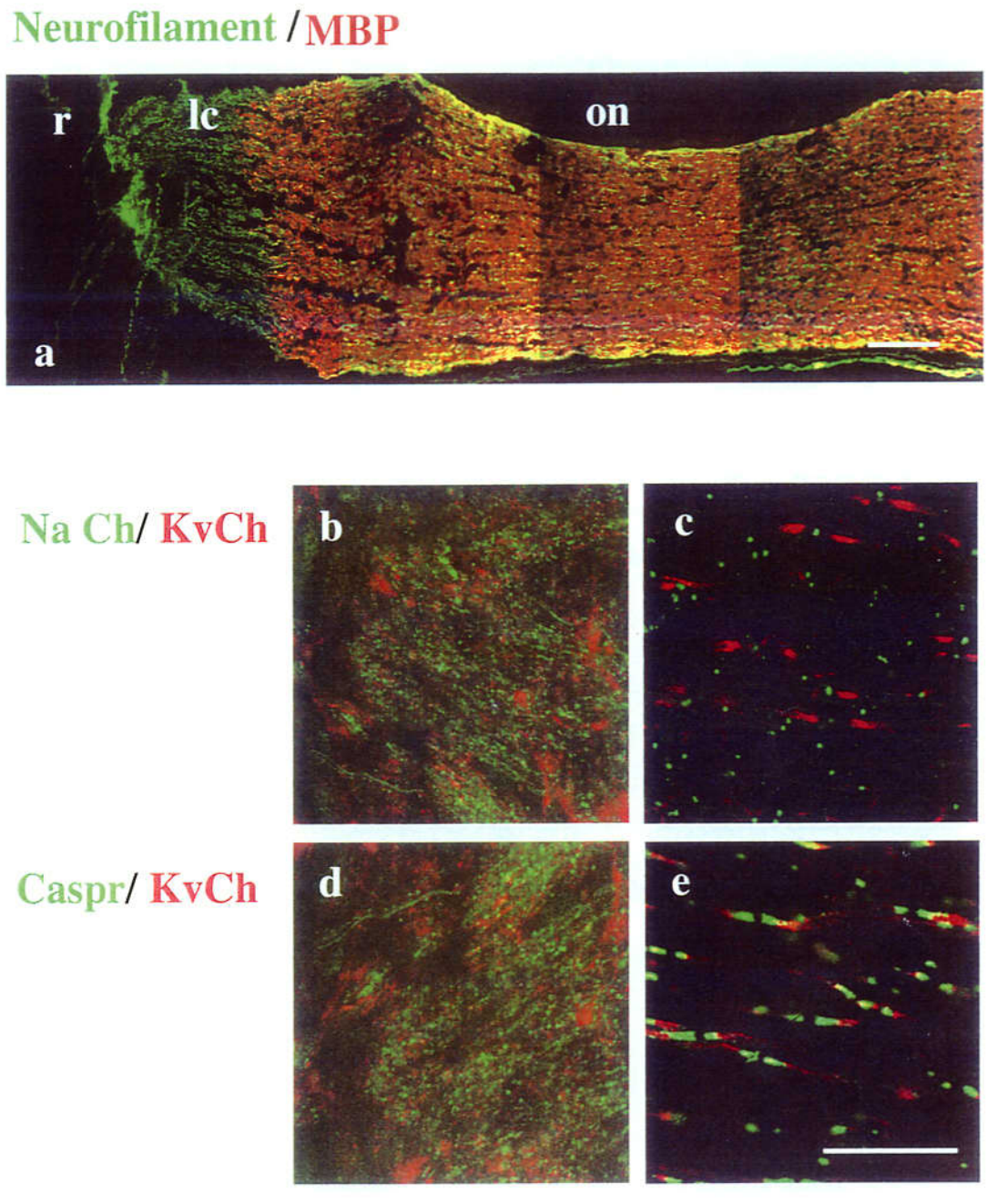

Figure 2

Myelinated and unmyelinated regions in the adult optic nerve

Cryosections of adult mouse optic nerve were double immunostained. The antibodies and the corresponding fluorescence colors are indicated in each panel. a) Neurofilament was detected throughout the axons, while anti-MBP staining (red) marked only the myelinated region of optic nerve (on). The transitional zone from unmyelinated to myelinated regions was clearly distinguished at the lamina cribrosa (lc). The retina was marked by r. (b-e) Double immunostaining patterns of Na^+ and K^+ channels (KvCh) (b, c) or Caspr and K^+ channels (d, e) were performed in unmyelinated (b, d) and myelinated (c, e) regions of optic nerve. b) Diffuse but strong immunoreactivities for both Na^+ (green) and K^+ (red) channels were observed in the unmyelinated regions. c) Na^+ channels (green) were restricted to the nodes of Ranvier, whereas K^+ channels (red) were concentrated in the juxtaparanodes. Anti-Caspr (green) staining was uniform in the unmyelinated region (d) and clustered at the paranode adjacent to K^+ channels (red) at the juxtaparanode in the myelinated optic nerve (e). Scale bar: (a) 250μm, (b-e) 10 μm.

Figure 3g

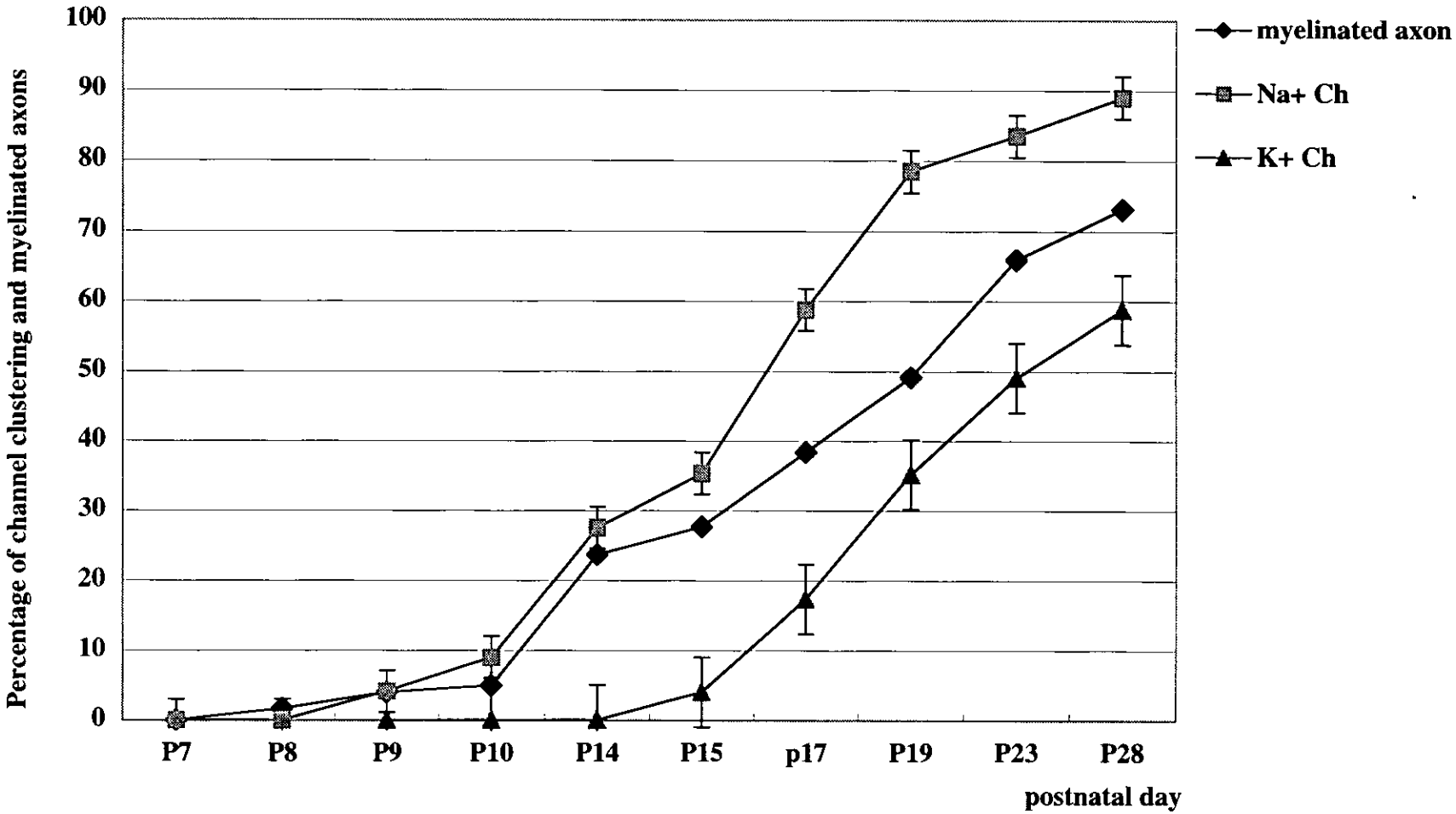
Percentage of channel clustering and myelinated axons
100
90
80
70
60
50
40
30
20
10
0
P7
P8
P9
P10
P14
P15
p17
P19
P23
P28
postnatal day
myelinated axon
Na+ Ch
K+ Ch

Figure 3

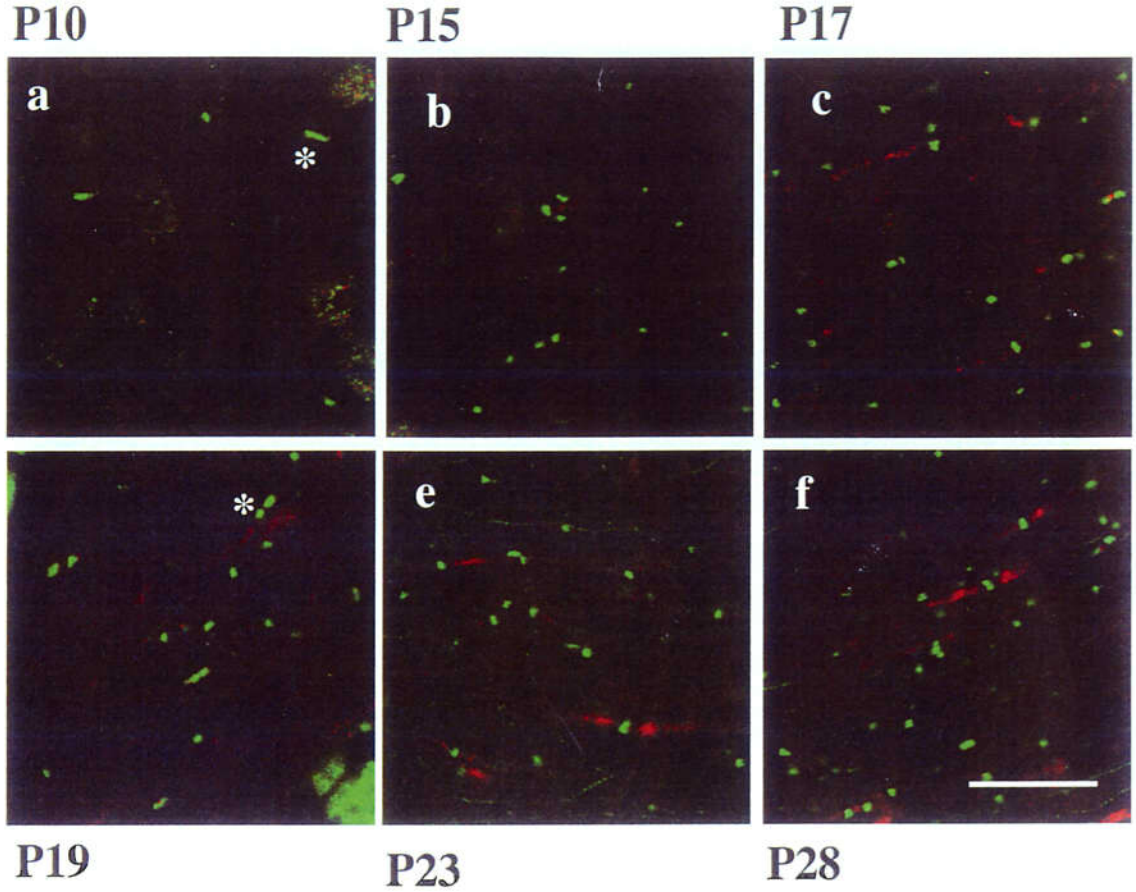

Figure 3

Distribution of Na^+ and K^+ channels in the developing mouse optic nerve

a-f) Optic nerve sections from postnatal day 10 (P10) to P28 double-labeled for Na^+ channels (green) and K^+ channels (red). a) Only a few Na^+ channel clusters were detected, but no K^+ channel clusters were observed at P10. b) At P15, Na^+ channel clustering was observed more frequently, but K^+ channels were still not detected. Between P15 (b) and P19 (c) Na^+ channel clusters increased dramatically, and K^+ channel clusters were occasionally detected near the Na^+ channel clusters from P17. e, f) Most of the Na^+ channel clusters were formed by P28, while K^+ channel clusters still increased and presented at both sides of Na^+ channel clusters. During early development (a-d) Na^+ channel clusters exhibited irregular shapes such as broad (a, asterisk, > 1.2μm) or binary-shape (d, asterisk). Scale bar: 10 μm. g) The correlation of myelination and channel cluster formation. The numbers of myelinated and unmyelinated axons were counted by electron microscopy, and percentage of myelinated axons in the total axons were plotted (◆). The numbers of Na^+ channel clusters (■) and K^+ channel clusters (▲) per field of view (FOV; 1FOV=73.1X73.1μm^2) were counted and the percentage of each channel clustering as a proportion of the numbers of adults was plotted. An average of 10 FOVs was analyzed at each age. Error bars represented SD.

Figure 4

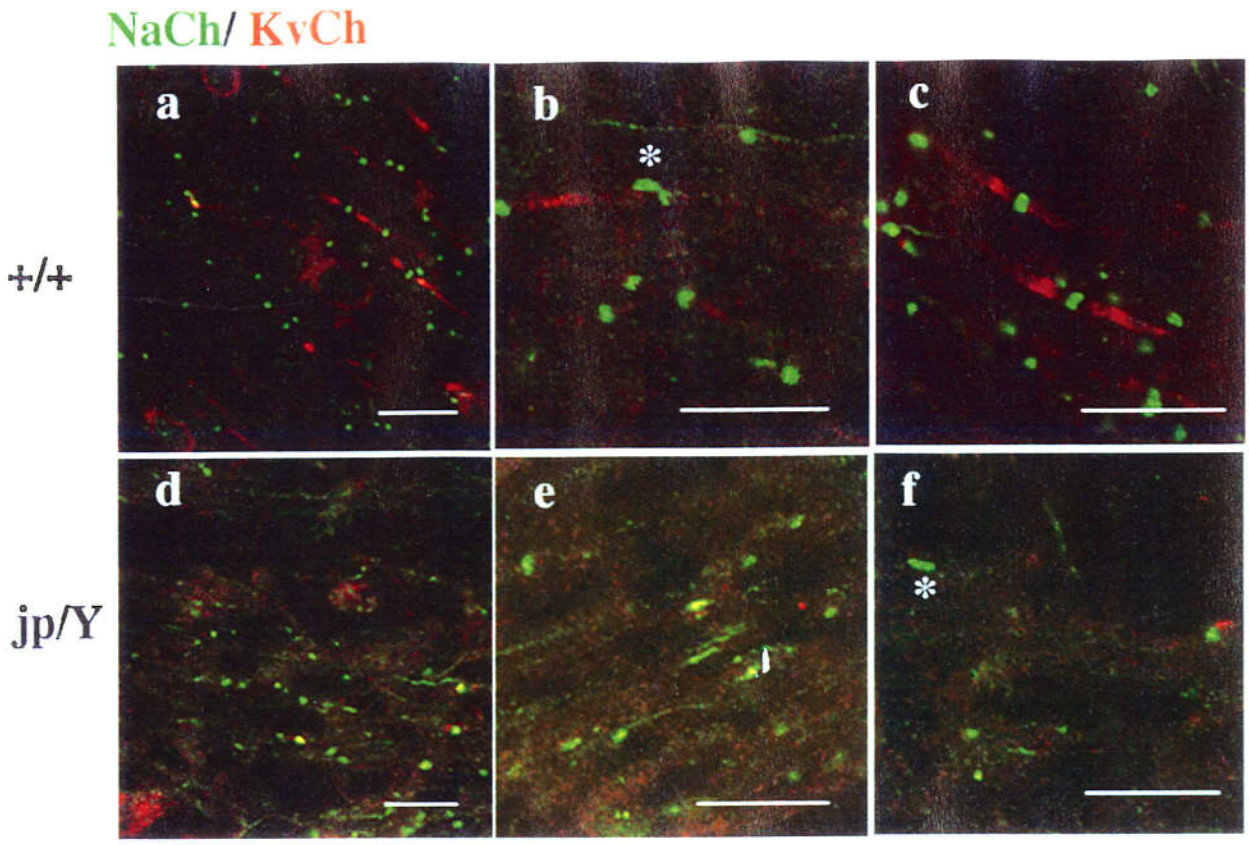

Figure 5

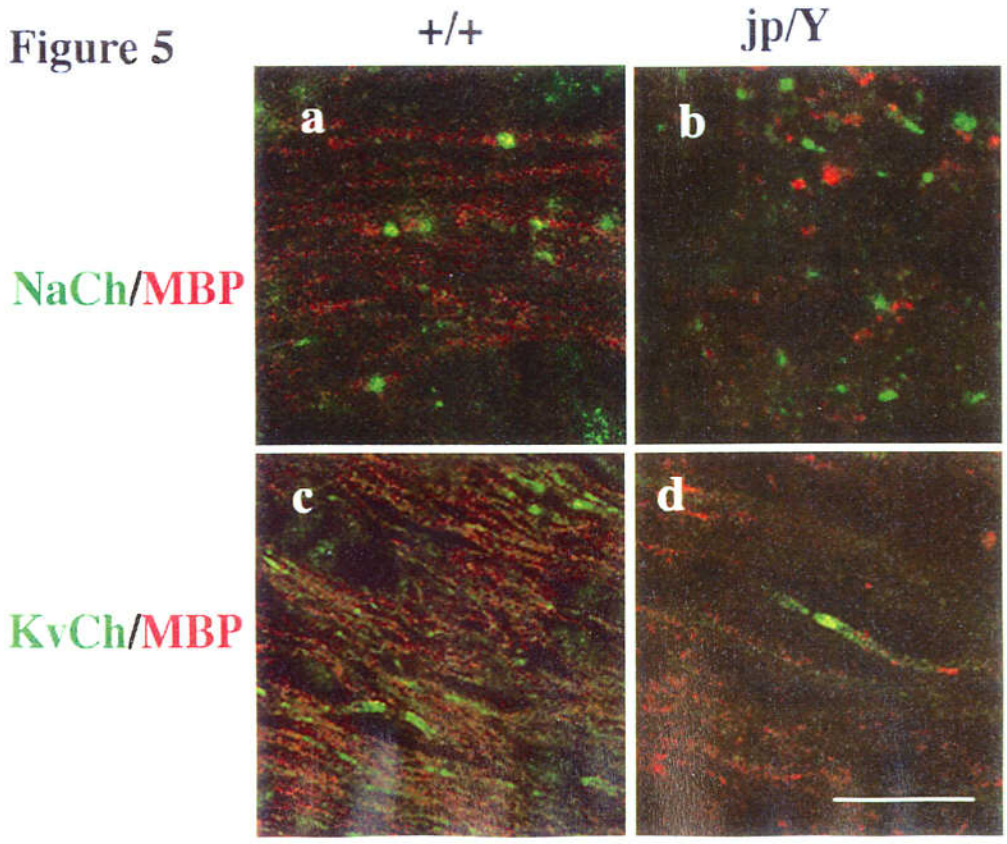

Figure 4

Localization of Na^+ and K^+ channels in hypomyelinating axons

Sections from the optic nerve of wild type (a-c) or *jimpy* (d-f) littermates at P21 were examined by double-immunostaining with antibodies against the Na^+ channels and K^+ channels. Three representative pictures of each mouse were demonstrated. In wild type mice (a-c), Na^+ channels (green) were restricted to the nodes of Ranvier, whereas Kv1.1 (red) were concentrated in the juxtaparanodes. A small number of broad Na^+ channel clusters were still observed at this age (b, asterisk). In *jimpy* mice, Na^+ channel clusters were observed (d), although the shapes of the clusters were irregular, such as broad (e) and binary shape (f, asterisk). K^+ channels distributed diffusely and no apparent clusters were observed in this mutant (d-f). Scale bar: 10 μm.

Figure 5

Localization of Na^+ and K^+ channels and MBP-positive myelin membranes in hypomyelinating axons

The optic nerves from *jimpy* mice (b, d) and wild type littermates at P21 (a, c) were double-immunostained with anti-MBP and anti- Na^+ channel (a, b) or anti-MBP and anti- Kv1.1 (c, d). In wild type mice (a, c), Na^+ channel (a, green) or K^+ channel (c, green) staining was concentrated either at the node or juxtaparanode, respectively, in MBP-positive myelinated fibers. In *jimpy* mice, the presence of Na^+ channel clusters were found in MBP-negative fibers (b), while K^+ channels formed clusters only in the MBP-positive myelinated fibers (d). Scale bar: 10 μm.

Figure 6 NaCh/Caspr

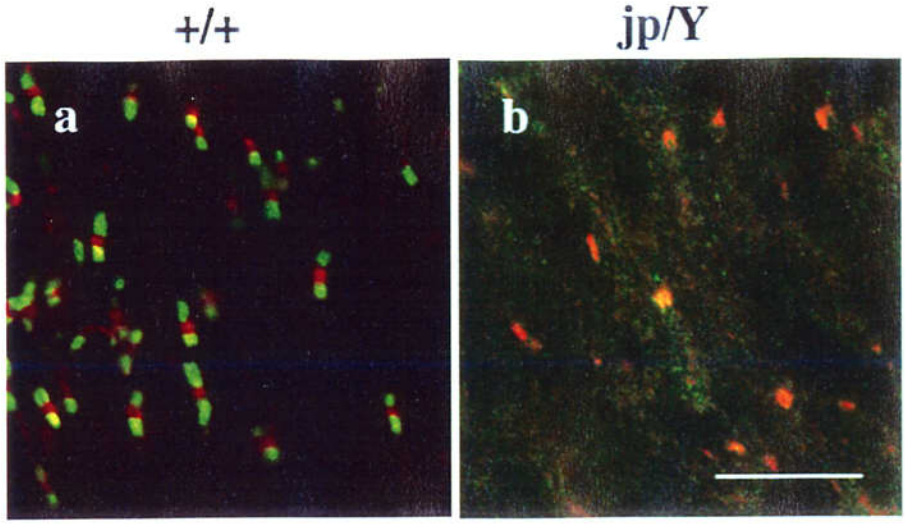

Figure 7

AnkyrinG/NaCh

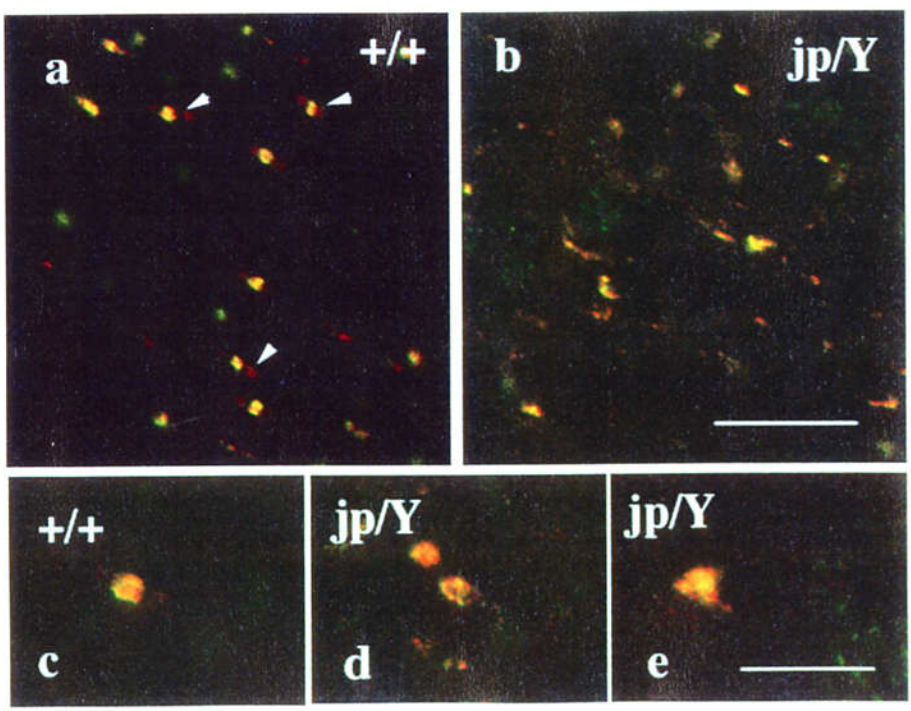

Figure 6

Distribution of Caspr in hypomyelinating axons

Sections from the optic nerves from *jimpy* (b) and wild type littermates (a) at P21 were examined by double-immunostaining with antibodies against Na^+ channels (red) and Caspr (green). In wild type (a), Caspr immunoreactivity (green) was restricted in the paranode, in most cases, flanking both sides of the nodal Na^+ channel clusters (red). In *jimpy* mice (b), Caspr immunoreactivity was diffusely distributed without any identifiable clusters in contrast to Na^+ channel clusters (see also in Figure 4). Scale bar: 10 μm.

Figure 7

Localization of Ankyrin$_G$ in hypomyelinating axons

Sections from optic nerves from *jimpy* (b, d, e) and wild type littermates (a, c) at P21 were examined by double-immunostaining with antibodies against ankyrin$_G$ (red) and Na^+ channels (green). In wild type (a, c), ankyrin$_G$ immunostaining always colocalized with Na^+ channels at the nodes. Additionally, weak immunoreactivity was also observed in the paranodal regions (a, arrow), which was probably due to the presence of another ankyrin family protein. In *jimpy* mice, ankyrin$_G$ clusters also colocalized with Na^+ channels, even though these clusters were occasionally represented by irregular shapes (d, e). Scale bar: 10 μm (a, b), (c-e) 5 μm.

Figure 8

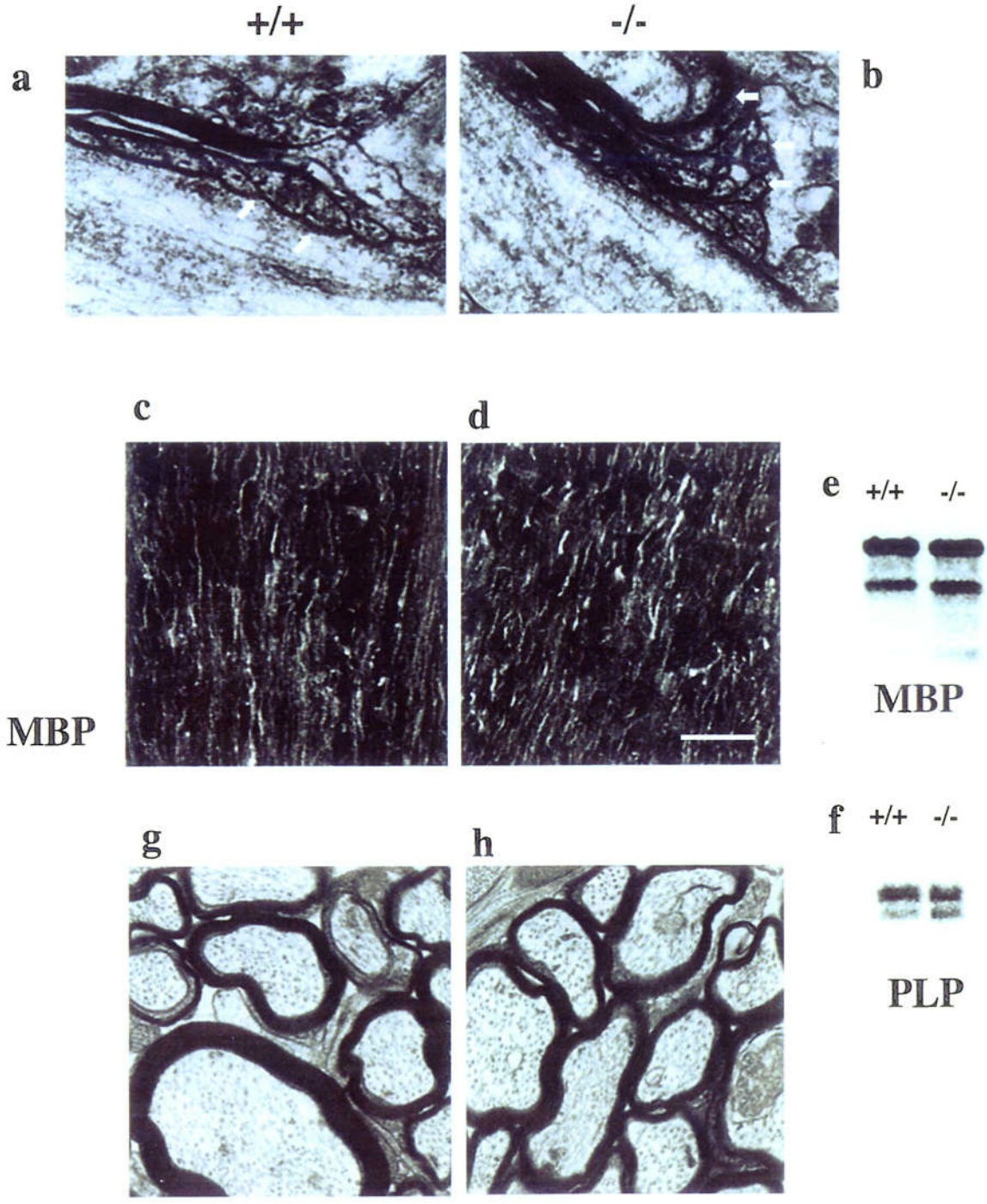

Figure 8

Myelin and paranodal morphology in wild type and CST-deficient mice

a, b) Perturbation of the paranodal organizaion of CST-deficient mice. Electron micrographs at the paranodal region of wild type (a) and the mutant mouse cerebellum at 13 weeks of age (b). In wild-type mice, the terminal loops were tightly attached to the axolemma at the paranode (a, arrows). (b) The paranodal region in CST-deficient mice represented everted paranodal loops and disappearance of the junctions (arrows). The staining patterns of MBP exhibited no differences between wild type (c) and CST-deficient (d) mice in optic nerves at 22 weeks of age. Scale bar: 10 μm. Western blot analysis of brain membrane fractions from wild type (+/+) and mutant (-/-) mice revealed no differences in the levels of MBP (e) and PLP (f) at 18 weeks of age. (g, h) Cross sectional analysis of optic nerves from 29-week old wild type (g) and CST-deficient (h) mice revealed no difference in compact myelin.

Figure 9 NaCh/KvCh

spinal cord

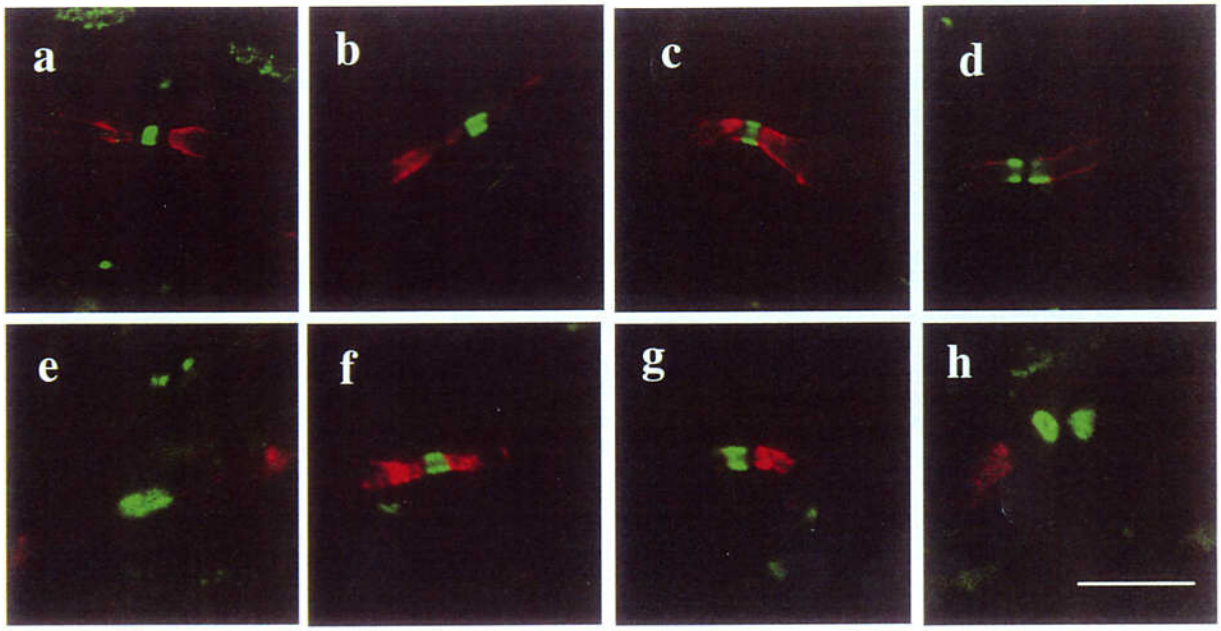

optic nerve

Figure 10 Caspr/KvCh

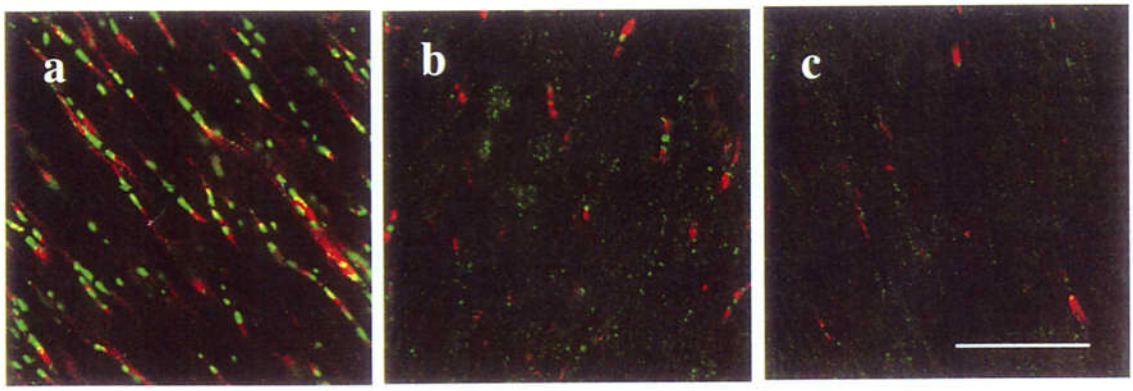

NaCh/Caspr

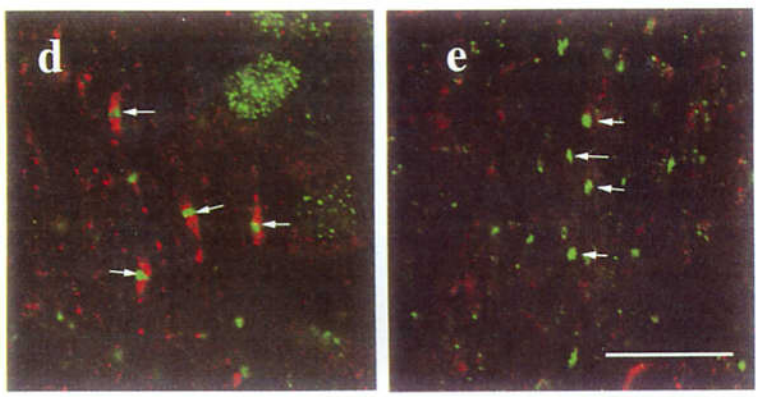

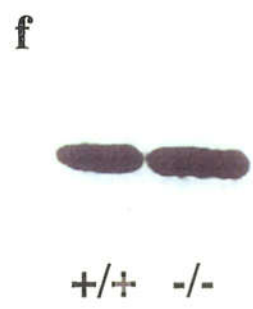

Figure 9 i

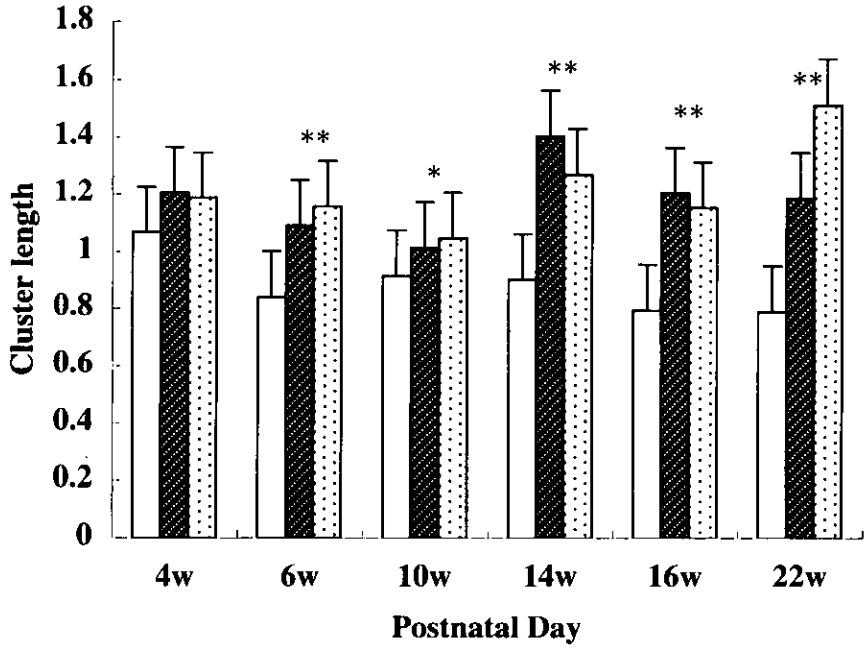
1.8
1.6
1.4
1.2
1
0.8
0.6
0.4
0.2
0
Cluster length
**
*
**
**
**
4w
6w
10w
14w
16w
22w
Postnatal Day

Figure 9

Alteration of ion channel clusters in CST-deficient mice.

Double immunostaining of Na^+ (green) and K^+ (red) channels was performed in the cryosections of spinal cords (a-d) and optic nerves (e-h). (a) In the spinal cord of wild-type mice, Na^+ channels (green) were restricted to the node, whereas K^+ channels (red) were concentrated in the juxtaparanode. In CST-deficient mice, the K^+ channels were aberrantly localized at the paranodes both in the spinal cord (b, c, d) and optic nerve (f). Na^+ channels formed clusters at the nodes, however, such Na^+ channel-positive domains were significantly longer (b, e, f) in comparison to those in wild type (a). (d, h) Binary form of sodium channel clusters was also observed. (g) Heminodal formation that labeled just one side of the juxtaparanode and/or paranode with the Kv1.1 antibody was observed. Scale bar: 10 μm. (i) The nodal lengths in the optic nerves of wild type (white bars) and the two mutant animals (oblique and white dotted bars), those were revealed by Na^+ channel immunoreactivity. Error bars indicate SD. (**) and (*) indicate $P < 0.001$ and $P < 0.05$, respectively.

Figure 10

Caspr clustering was severely disrupted in CST-deficient mice

(a) In 6-week-old wild type mice, Caspr (green) was highly concentrated in paranodal regions of the optic nerve. (b, c) In contrast, CST-deficient mice at 6w (b) and 10w (c) of age exhibited more diffuse distribution of Caspr. The number of K^+ channel clusters was markedly decreased in the mutant optic nerves (b, c). (d, e) CST-deficient mice exhibited severe disruptions in Caspr cluster formation during development (P17) as well. Optic nerve sections from control littermates (d) and CST-deficient mice (e) were double-labeled to indicate the localization of Na^+ channel (green) and Caspr (red). Caspr clustering was hardly observed and this protein was distributed diffusely along the axons in CST-deficient mice (e). In contrast, Na^+ channel cluster formation was comparable between mutants (e, arrow) and control littermates (d, arrow). Scale bar: 10 μm. (f) Western blot analysis of brain homogenate revealed no differences in the amount of Caspr protein between wild type (+/+) and mutant (-/-) mice in the CNS axons at 18 weeks of age.

Figure 11 NaCh/KvCh

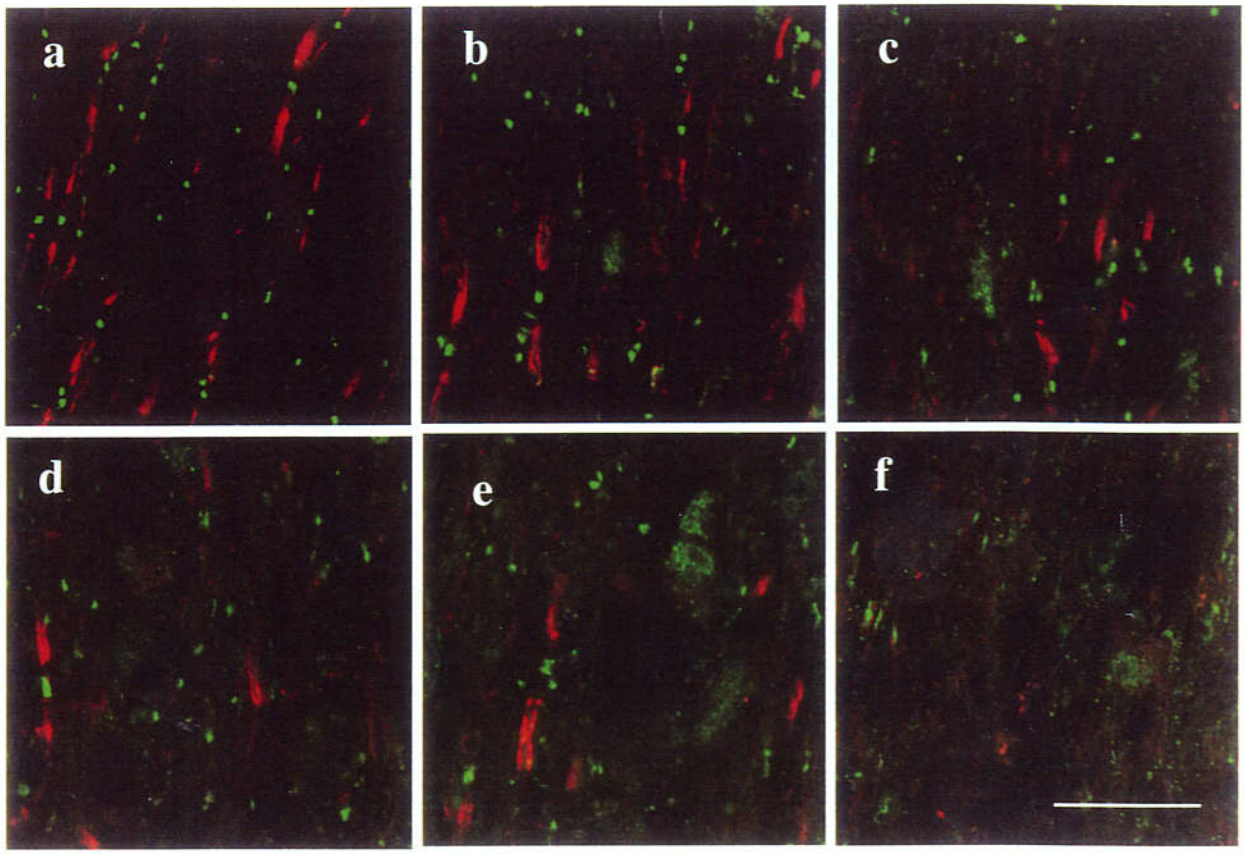

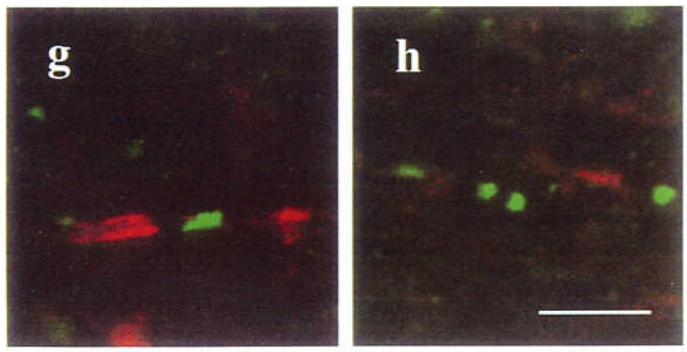

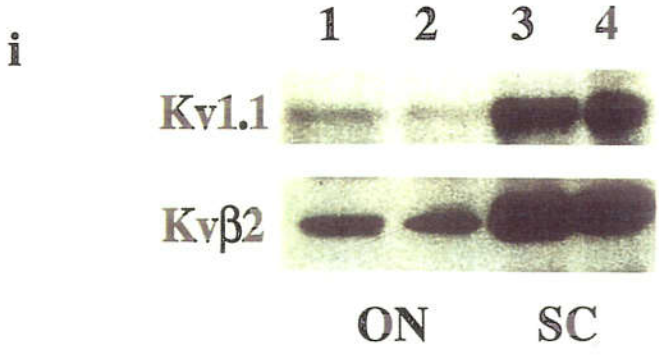

Figure 11 j

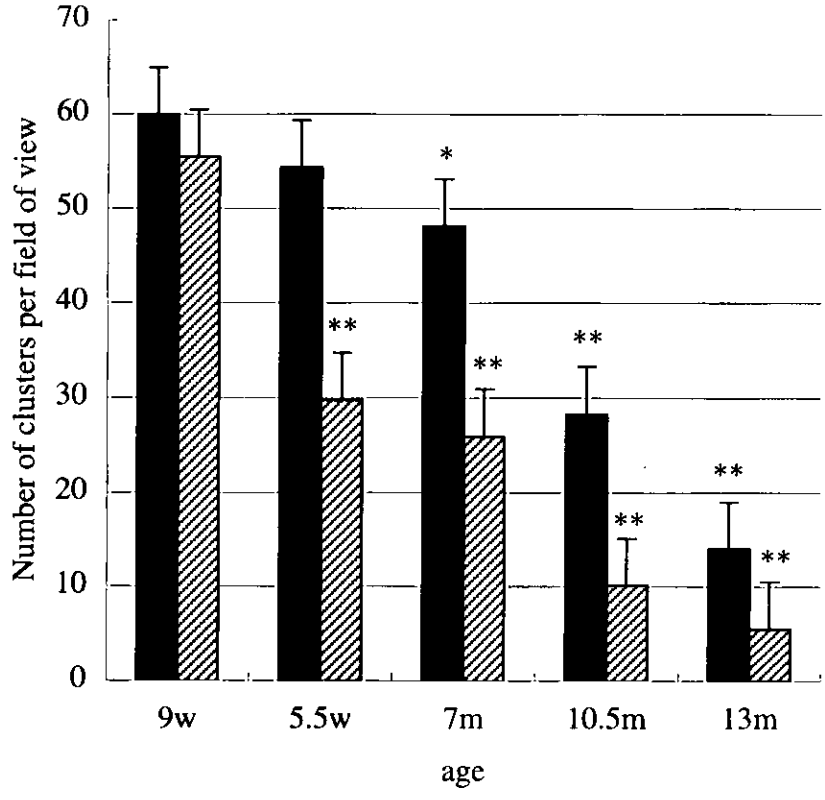
70
60
50
40
30
20
10
0
Number of clusters per field of view
*
**
**
**
**
**
9w
5.5w
7m
10.5m
13m
age

Figure 11

Both Na^+ and K^+ channel clusters were reduced during demyelination in PLP transgenic (*tg*) mice.

The optic nerves from mice at ages of 9w (a), 5.5 months (m) (b, c), 7m (d), 10.5m (e), and 13m (f) were double-immunostained by Na^+ (green) and K^+ (red) channel antibodies. At 9w of age (a), the numbers of Na^+ (green) and K^+ (red) channel clusters in PLP *tg* were comparable to those in wild-type (data not shown). At 5.5m (b, c), 7m (d), 10.5m (e) of age, K^+ channel clusters were markedly reduced and such changes became more prominent with age. In contrast, Na^+ channel clusters decreased much more slowly (b-e). At 13m of age (f), both of Na^+ and K^+ channels were barely detectable. (g, h) Some of the remaining Na^+ channel clusters at 5.5m of age revealed irregular shapes, such as broad (g) and binary-shape (h). Scale bar, 10 μm (a-f), 5 μm (g, h). (i) The protein levels of K^+ channel α and β subunits were examined by Western blot analysis. The optic nerves (on) and spinal cords (sc) from transgenic (lane 1, 3) or wild type (lane 2, 4) animals were homogenized and separated by 7.5% SDS-PAGE. The blots were stained by antibodies against Kv1.1 and Kvβ2. Although the channel clusters reduced significantly with age (b-f), the protein levels of these subunits in demyelinated axons were comparable to those in wild type mice. (j) Numbers of Na^+ channel (black bars) and K^+ channel (oblique bars) clusters per FOV were counted in the optic nerves from PLP *tg* mice of different ages. An average of 12 FOVs were analyzed at each age. Error bars indicate SD. (**) and (*) indicate $P < 0.001$ and $P < 0.02$, respectively.

Table 1

Summary of the changes of voltage-gated ion channel clusters on the axons under several myelin conditions

myelin conditions	**Voltage-gated Na+ channel clustering**	**Voltage-gated K+ channel clustering**
Unmyelinated axons oligodendrocyte (-) compact myelin (-) paranodal junction (-)	-	-
Hypomyelination O1+oligodendrocyte (+) compact myelin (-) paranodal junction (-)	mature clusters < 30% immatre clusters > 70%	-
Paranodal disruption oligodnedrocyte (+) compact myelin (+) paranodal junction (-)	mature clusters < 50% immature clusters (broad form > 50%) (binary shape ~12%)	presumptive paranode > paranode
Myelinated axons oligodendrocytes (+) compact myelin (+) paranodal junction (+)	mature clusters 100% immature clusters (appear only during development)	juxtaparanode
Chronic demyelination oligodendrocyte (+)→(-) compact myelin (+)→(-) paranodal junction (+)→(-)	mature clusters decrease gradually	dissapear immediately

Chapter II

Figures and Figure legends

Figure 1 CD9 /Caspr

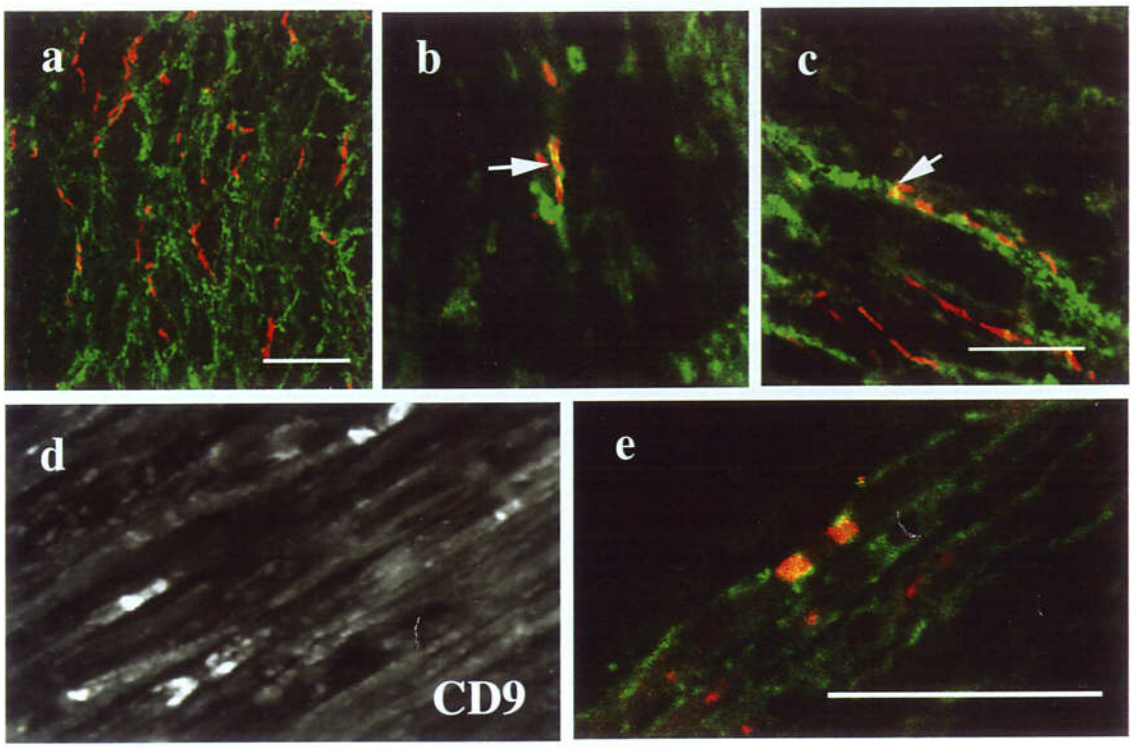

Figure 2

CD9

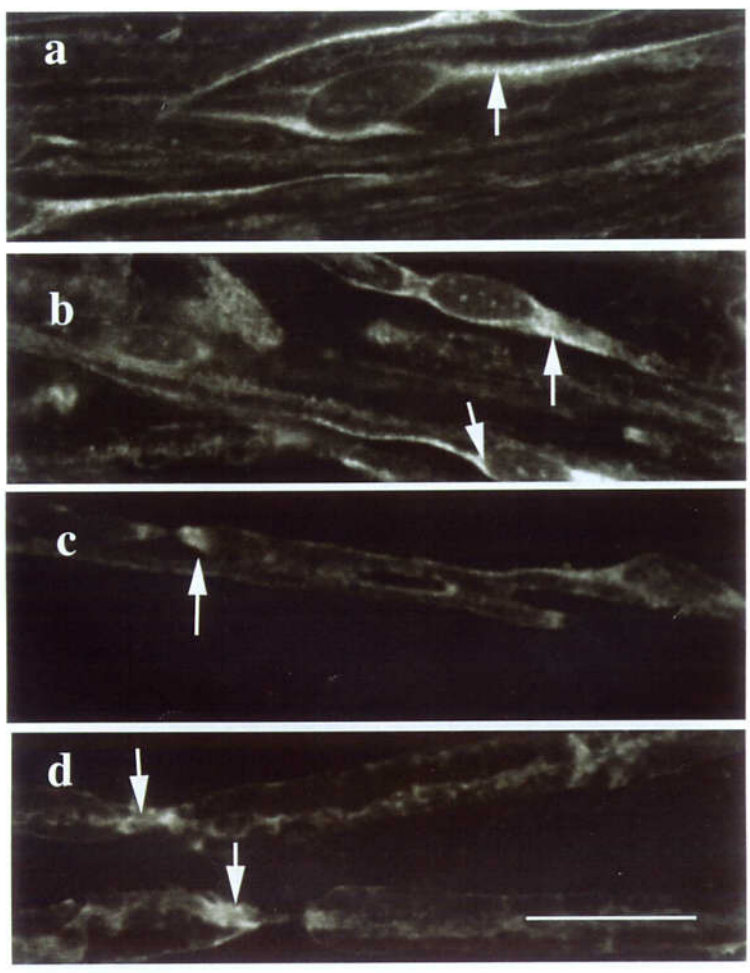

Chapter II

Figure 1

CD9 (green) and Caspr (red) colocalized at the axo-glial junction both in the CNS and PNS.

(a-c) In adult optic nerve, CD9 (green) and Caspr (red) were occasionally colocalized (b, c, arrow). (d) In adult sciatic nerve, CD9 staining displayed a pair of clusters as well as diffusely along myelin. (e) Doube staining for CD9 (green) and Caspr (red) showed overlap at the paranode (yellow). Scale bar, 10 μm.

Figure 2

Developmental profile of CD9 distribution in myelinated sciatic nerve

(a, b) At P0 and P1, CD9 was expressed just in the cell body of Schwann cells (arrow). (c) At P2, CD9 was expressed in presumptive paranode (arrow) as well as myelin surface. (d) At P4, CD9 was localized markedly at the paranode (arrow). Scale bar, 5 μm.

Figure 3

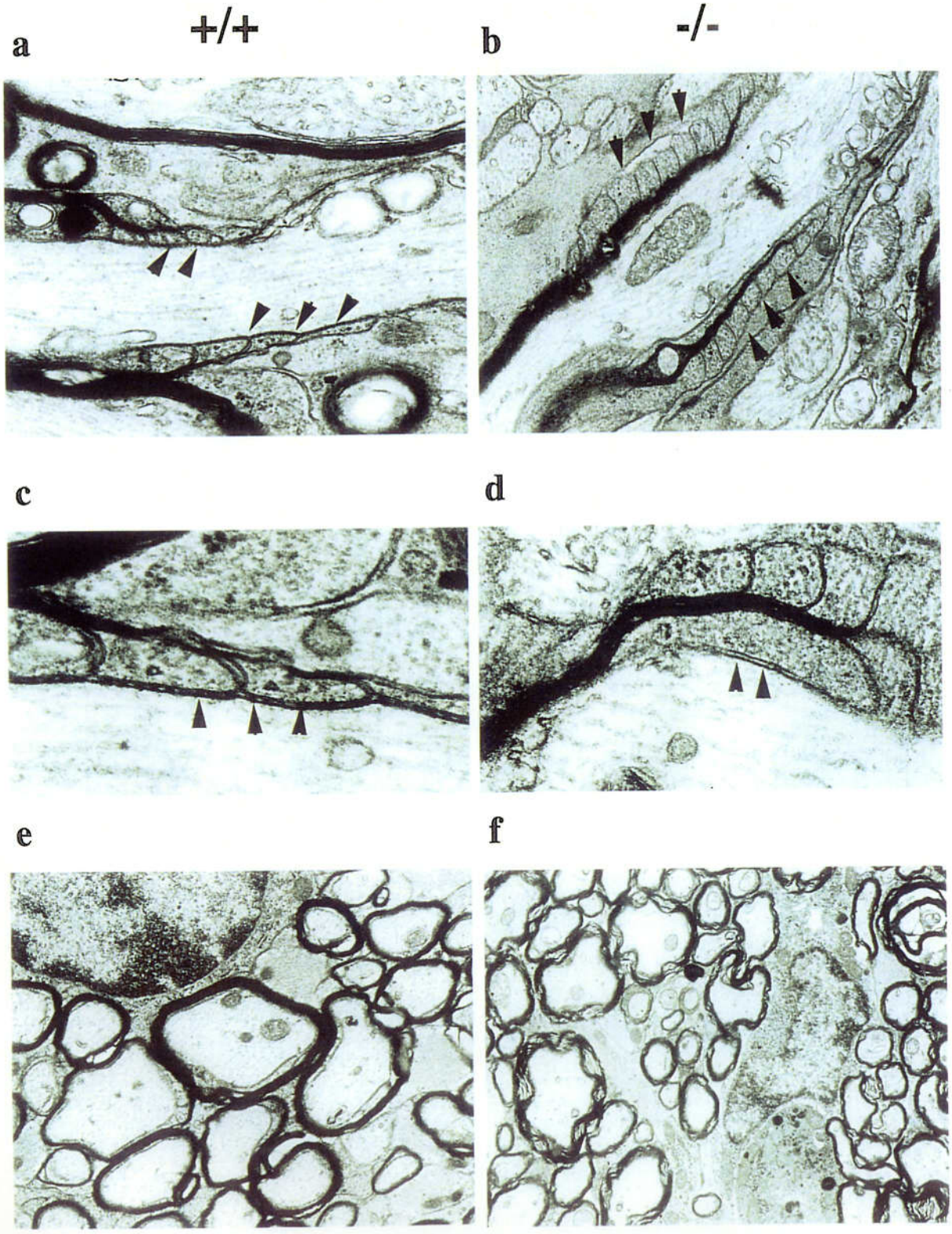

Figure 3

Myelin and paranodal morphology in wild-type and CD9-deficient mice

(a-d) Perturbation of the paranodal organizaion in optic nerve from CD9-deficient mice at 8 weeks of age. Electron micrographs through the paranodal region in optic nerve from wild type (a, c) and the mutant mice (b, d). In wild type, the terminal loops were tightly attached to the axolemma at the paranode (a, arrowheads), and the characteristic transverse bands were observed at higher magnification (c, arrowheads). (b) showed mutant paranodal region with everted paranodal loops and disruption of the junctions (arrowheads). (d) Only the paranodal loops of innermost myelin remained attached to the axon, but transverse bands were never observed (arrowheads). (e, f) Electron microscopic analysis showed no signs of demyelination. Cross sectional analysis of optic nerves from 8-week old wild type (e) and CD9-deficient (f) mice revealed no difference in compact myelin.

Figure 4

Na Ch/ KvCh

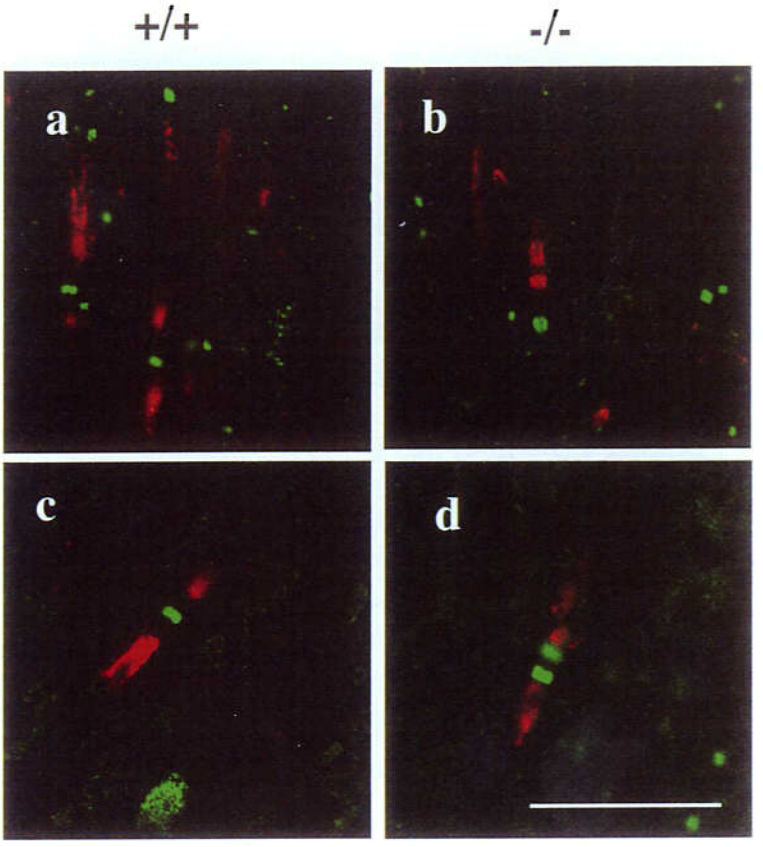

Figure 5 Caspr/ KvCh

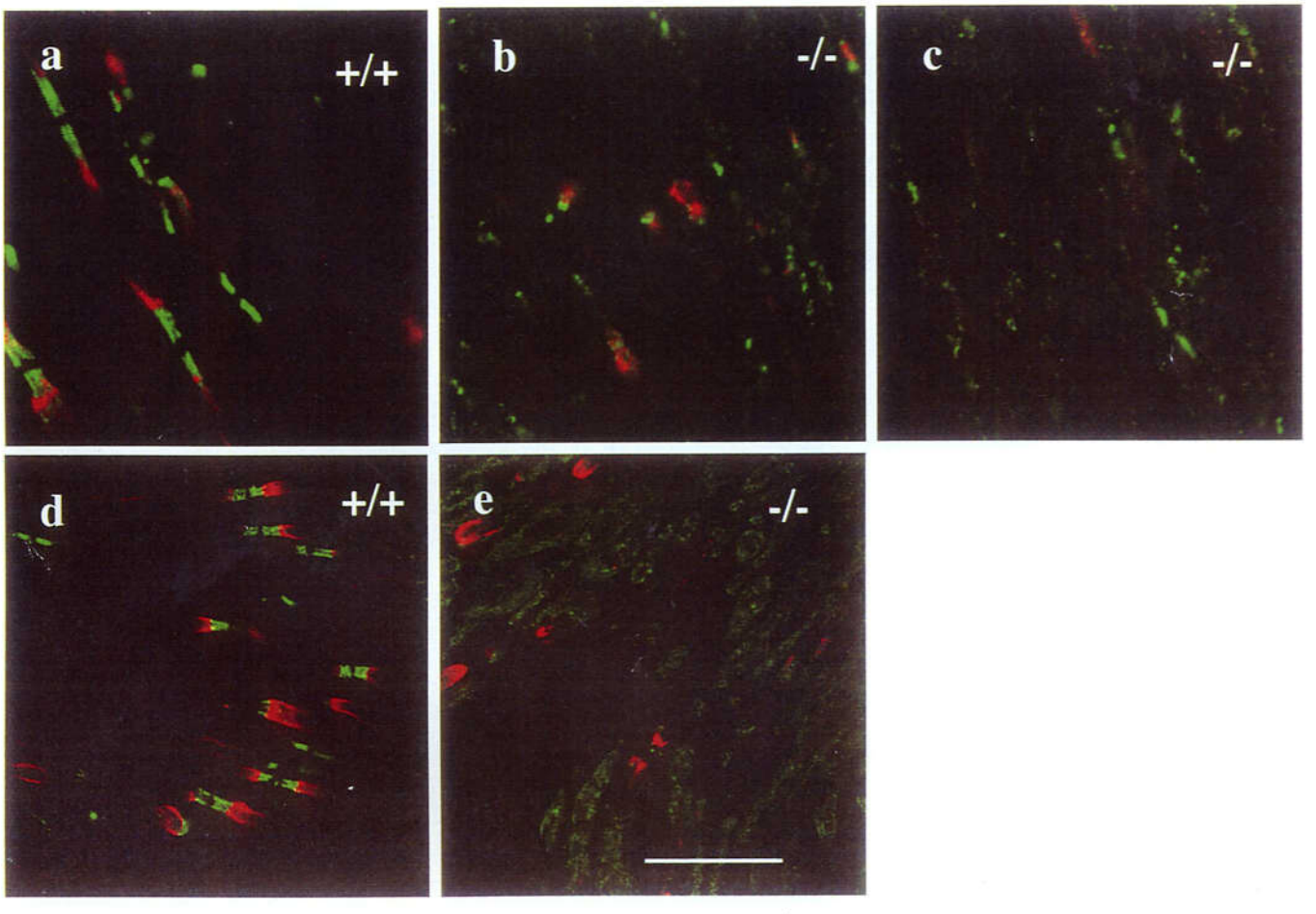

Figure 4

Ion channel distribution was altered in CD9-deficient mice

Double immunostaining of Na^+ (green) and Kv1.1 (red) channels was performed in the optic nerves (a, b) and spinal roots (c, d). Both in the optic nerve (a) and spinal root (c) of wild-type mice, Na^+ channels were restricted to the nodes of Ranvier, whereas K^+ channels were concentrated in the juxtaparanodes. In contrast, in CD9-deficient mice heminode formation that labeled just one side of either juxtaparanode or paranode with the Kv1.1 antibody was observed (b), the K^+ channels were also aberrantly localized at the paranode in the spinal root (d). The Na^+ channels formed clusters in the nodes, however, binary form of sodium channel clusters were observed (d). Scale bar: 10 μm.

Figure 5

CD9-deficient mice revealed severely disrupted Caspr clustering

Optic nerves (a-c) and spinal roots (d, e) from 8-week-old control littermates (a, d) and CD9-deficient mice (b, c, e) were double-labeled to indicate the localization of Kv1.1 channel (red) and Caspr (green). Caspr (green) was highly concentrated in the paranodal regions of the optic nerve (a) and spinal root (d). In contrast, CD9-deficient mice exhibited that Caspr was distributed diffusely and remaining clusters of Caspr were shown irregular shape (b, c). Caspr clustering was also hardly observed and this protein was distributed diffusely along the axons in spinal root of CD9-deficient mice (e). The number of K^+ channel clusters (red) in the both regions was decreased in the mutant (b, c, e). Scale bar: 10 μm

Figure 6

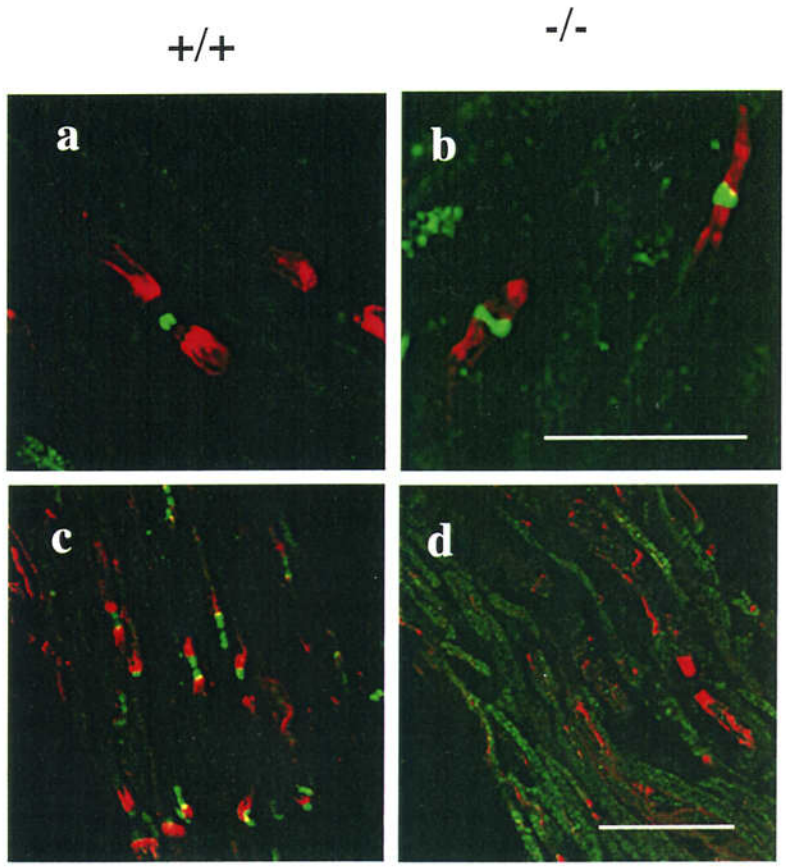

Figure 7

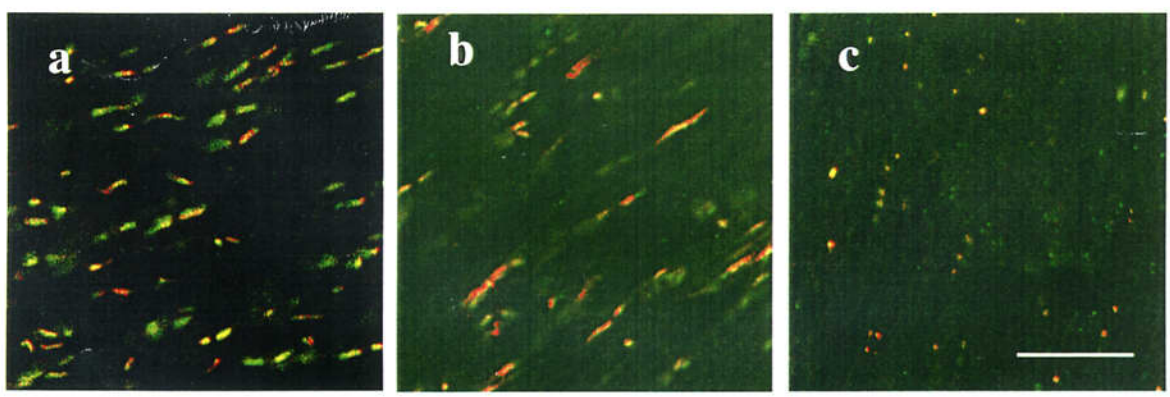

Figure 6

Altered distribution of axonal components in the PNS from CST-deficient mice

Spinal roots from control littermates (a, c) and CST-deficient mice (b, d) were double-labeled by the antibodies against either Na^+ channels (green) and K^+ channels (red) (a, b) or Caspr (green) and K^+ channels (red) (c, d). (a, c) In wild-type mice, Na^+ channels (green in a) were restricted to the nodes of Ranvier, whereas K^+ channels (red in a and c) were concentrated in the juxtaparanodes as described, previously. Caspr was concentrated in the paranode (green in c). (b, d) In contrast, in CST-deficient mice, the K^+ channel clusters were aberrantly localized at the paranodes and occasionally overlapped with Na^+ channels (b, yellow). Caspr was distributed diffusely and the cluster was never observed (d). Scale bar: 10 μm.

Figure 7

Distribution of NF155 was also changed in both mutants with paranodal abnormality

Double immunostaining of NF155 (green) and Caspr (red) was performed in the optic nerves of wild type (a), CD9-deficient (b), and CST-deficient (c) mice. (a) At 8 weeks of age in wild-type mice, NF155 and Caspr were colocalized at the paranode. (b) At 8 weeks of age in CD9-deficient mice, NF155 was distributed diffusely, nevertheless, the remaining clusters of NF155 and Caspr were always colocalized. (c) At 10 weeks of age in CST-deficient mice, NF155 was hardly detected in the paranodal regions but instead was concentrated in discrete patches where it frequently colocalized with Caspr. Scale bar: 10 μm.